TRPM2 ion channels regulate macrophage polarization and gastric inflammation during *Helicobacter pylori* infection

S Beceiro[1], JN Radin[2], R Chatuvedi[2,8], MB Piazuelo[2], DJ Horvarth[2], H Cortado[1], Y Gu[3], B Dixon[2], C Gu[3], I Lange[4], D-LT Koomoa[4], KT Wilson[2,5,6], HMS Algood[2,5,6,9] and S Partida-Sánchez[1,7,9]

Calcium signaling in phagocytes is essential for cellular activation, migration, and the potential resolution of infection or inflammation. The generation of reactive oxygen species (ROS) via activation of NADPH (nicotinamide adenine dinucleotide phosphate)-oxidase activity in macrophages has been linked to altered intracellular calcium concentrations. Because of its role as an oxidative stress sensor in phagocytes, we investigated the function of the cation channel transient receptor potential melastatin 2 (TRPM2) in macrophages during oxidative stress responses induced by *Helicobacter pylori* infection. We show that *Trpm2*$^{-/-}$ mice, when chronically infected with *H. pylori*, exhibit increased gastric inflammation and decreased bacterial colonization compared with wild-type (WT) mice. The absence of TRPM2 triggers greater macrophage production of inflammatory mediators and promotes classically activated macrophage M1 polarization in response to *H. pylori*. TRPM2-deficient macrophages upon *H. pylori* stimulation are unable to control intracellular calcium levels, which results in calcium overloading. Furthermore, increased intracellular calcium in TRPM2$^{-/-}$ macrophages enhanced mitogen-activated protein kinase and NADPH-oxidase activities, compared with WT macrophages. Our data suggest that augmented production of ROS and inflammatory cytokines with TRPM2 deletion regulates oxidative stress in macrophages and consequently decreases *H. pylori* gastric colonization while increasing inflammation in the gastric mucosa.

INTRODUCTION

The regulation of calcium (Ca^{2+}) influx across the plasma membrane is crucial for phagocyte activation and phagocyte-mediated immune responses. Cytosolic levels of Ca^{2+} control a diverse range of cellular processes, including chemotaxis, adhesion, phagocytosis, and the secretion of pro- and anti-inflammatory cytokines in phagocytic cells.[1,2] In addition to the main channels responsible for Ca^{2+} entry, the store-operated Ca^{2+} release-activated Ca^{2+} channels [3] and some members of the transient receptor potential (TRP) channel superfamily (TRPM2, TRPM4, TRPM7, TRPV2, TRPC1) are indispensable components in the regulation of Ca^{2+} homeostasis significantly impacting the function of macrophages.[4,5]

Transient receptor potential melastatin 2 (TRPM2) is a nonselective, Ca^{2+}-permeable cation channel with an adenosine diphosphate ribose (ADPR) pyrophosphatase enzymatic NUDIX site at the C-terminus domain.[6–8] TRPM2 is activated upon the direct binding of intracellular ADPR[6,7] and indirectly under conditions of oxidative stress via the formation of hydrogen peroxide (H_2O_2), and thus can function as an oxidative stress sensor.[9–11] TRPM2 is highly expressed in specialized phagocytic cells.[8,12,13] Phagocytes expressing

[1]Center for Microbial Pathogenesis, The Research Institute at Nationwide Children's Hospital, Columbus, Ohio, USA. [2]Department of Medicine, Vanderbilt University School of Medicine, Nashville, Tennessee, USA. [3]Department of Neuroscience, College of Medicine, The Ohio State University, Columbus, Ohio, USA. [4]The Daniel K Inouye College of Pharmacy, University of Hawaii at Hilo, Hilo, Hawaii, USA. [5]Tennessee Valley Healthcare System, Department of Veterans Affairs, Nashville, Tennessee, USA. [6]Department of Pathology, Microbiology and Immunology, Vanderbilt University School of Medicine, Nashville, Tennessee, USA and [7]Department of Pediatrics, College of Medicine, The Ohio State University, Columbus, Ohio, USA. Correspondence: HMS Algood or S Partida-Sanchez (holly.m.algood@vanderbilt.edu or Santiago.Partida-Sanchez@nationwidechildrens.org)
[8]Current address: School of Biotechnology, Jawaharlal University, New Delhi, India.
[9]These authors contributed equally to this work.

Received 15 January 2016; accepted 9 June 2016; published online 20 July 2016. doi:10.1038/mi.2016.60

TRPM2 respond to reactive oxygen species (ROS) secreted at inflammatory sites by releasing cytokines and chemokines, which have essential roles in the outcome and resolution of inflammation, especially in mucosal tissues.[8,11,14]

Detailed characterization of TRPM2 genetically deficient mice in different inflammatory models has revealed the involvement of this channel in various aspects of innate immunity. In the dextran sulfate sodium-induced colitis model, *Trpm2*$^{-/-}$ mice were less susceptible to tissue ulceration.[8] In inflammatory and neuropathic pain models, *Trpm2*$^{-/-}$ mice displayed an impaired cellular infiltration.[15] In contrast, *Trpm2*$^{-/-}$ mice are more vulnerable to infection with *Listeria monocytogenes* than wild-type (WT) mice.[16] Di *et al.*[11] proposed that TRPM2 protects mice in an endotoxin-induced lung inflammation model through inhibition of the membrane NADPH (nicotinamide adenine dinucleotide phosphate)-oxidase complex in phagocytic cells. The diversity of these findings suggests that TRPM2 may have distinct roles under different inflammatory situations. It is therefore important to clarify the mechanisms by which TRPM2 activation may exert a pro- or anti-inflammatory function in mucosal tissues.

Many bacterial infections stimulate NADPH-oxidase activity in phagocytes to produce a burst of superoxide anions (O_2^-) that are converted into H_2O_2, which contributes to oxidative stress and the development of inflammation. *Helicobacter pylori* infection of the gastric mucosa triggers a vigorous innate and adaptive immune response characterized by local increase of oxidative stress, and the accumulation of polymorphonuclear leukocytes, macrophages, and lymphocytes.[17] Both the immune response and the bacterium itself contribute to the elevated levels of ROS and reactive nitrogen species within the infected gastric mucosa.[18] Moreover, excessive oxidative and nitrosative stress within the *H. pylori*-infected gastric mucosa correlate with mucosal damage and bacterial burden. The induction of inducible nitric oxide synthase (iNOS) and NADPH-oxidase responses by *H. pylori* in the gastric mucosa provide an ideal milieu to test the ability of the oxidative stress-activated cation channel TRPM2 to regulate the immune response to *H. pylori*.

This study investigated how TRPM2-mediated functions affect the immune response and pathogenesis of chronic *H. pylori* infection in a mouse model. Our findings reveal that *H. pylori* activate TRPM2 in macrophages. However, the loss of TRPM2 results in increased *H. pylori*-induced gastritis and decreased bacterial colonization in mice. Importantly, chronically *H. pylori*-infected *Trpm2*$^{-/-}$ mice exhibit augmented inflammatory cytokine production, enhanced NADPH-oxidase activity, and increased macrophage recruitment compared with *H. pylori*-infected WT mice. The absence of TRPM2 in macrophages results in enhanced production of ROS and activation of mitogen-activated protein kinases (MAPKs) in response to *H. pylori*. TRPM2$^{-/-}$ macrophages show increased baseline and *H. pylori*-induced intracellular Ca^{2+} levels compared with WT macrophages. Our findings suggest that TRPM2 mediates Ca^{2+} homeostasis and plasma membrane currents that are essential in regulating NADPH activity. Moreover, TRPM2 impacts the production of ROS and inflammatory cytokines, which subsequently mediate the gastric colonization and inflammatory damage of the gastric mucosa during *H. pylori* infection.

RESULTS

TRPM2 deficiency favors inflammatory profile and M1 macrophage polarization

Macrophages polarize to classically activated (M1) macrophages by bacterial stimulation or to alternatively activated (M2) macrophages by parasite infection, tissue remodeling, or tumor progression.[19,20] To determine whether TRPM2$^{-/-}$ bone marrow-derived macrophages (BMDM) can polarize toward classical or alternative macrophage activation *in vitro*, BMDM from WT and *Trpm2*$^{-/-}$ mice were treated with M1- (lipopolysaccharide (LPS) plus interferon-γ (IFN-γ)) or M2- (interleukin-4 (IL-4) plus IL-13) polarizing stimuli, and gene expression was assessed by quantitative real-time PCR (qRT-PCR). The combination of expression of the M1-associated markers, *Il6*, *Tnfa*, and *Nos2*, was significantly enhanced in TRPM2$^{-/-}$ macrophages compared with WT macrophages (**Figure 1a**). Furthermore, the absence of TRPM2 led to a significant reduction of the M2-specific marker *Arg1* compared with WT macrophages (**Figure 1a**). Furthermore, the production of NOS protein was markedly increased in TRPM2$^{-/-}$ when compared with WT BMDM, under M1-stimulating conditions. TRPM2$^{-/-}$ macrophages produced slightly increased NOS protein even under M2 stimulation (**Figure 1b**). In contrast, arginase 1 (Arg1) protein production was greater in WT as compared with TRPM2$^{-/-}$ BMDM, under M2-stimulating conditions (**Figure 1b**). Taken together, these data suggest that TRPM2$^{-/-}$ macrophages are refractory to M2 polarization or predisposed to polarize to M1-like subset regardless of stimulation. To determine whether TRPM2$^{-/-}$ BMDMs were prone to M1 polarization during differentiation in culture, we harvested unstimulated WT and TRPM2$^{-/-}$ macrophages after 7 days in culture, and then measured the relative mRNA levels of the M1-associated markers, *Il1b*, *Il6*, *Tnfa*, and *Nos2*. Neither M1 inflammatory cytokines nor *Nos2* were significantly elevated in unstimulated TRPM2$^{-/-}$ BMDM (**Supplementary Figure S1** online).

As the roles of ROS-sensitive TRPM2 during chronic inflammation are controversial, we next evaluated macrophage function during coculture with *H. pylori*, a bacterium that induces a strong oxidative response and activates gastric inflammatory response initiated by macrophages *in vivo*.[21,22] To assess the effects of TRPM2 deficiency on the production of inflammatory mediators by macrophages, we measured the expression levels of proinflammatory cytokines in WT and TRPM2$^{-/-}$ BMDMs cocultured with *H. pylori*, and compared it with uninfected controls, respectively. TRPM2$^{-/-}$ BMDM demonstrated a markedly enhanced expression of *Tnfa*, *Il6*, and *Il12p40* in response to *H. pylori* (**Figure 1c**). Having observed that *H. pylori*-infected *Trpm2*$^{-/-}$ mice showed increased expression of proinflammatory macrophage markers, we hypothesized that TRPM2$^{-/-}$ macrophages may exhibit

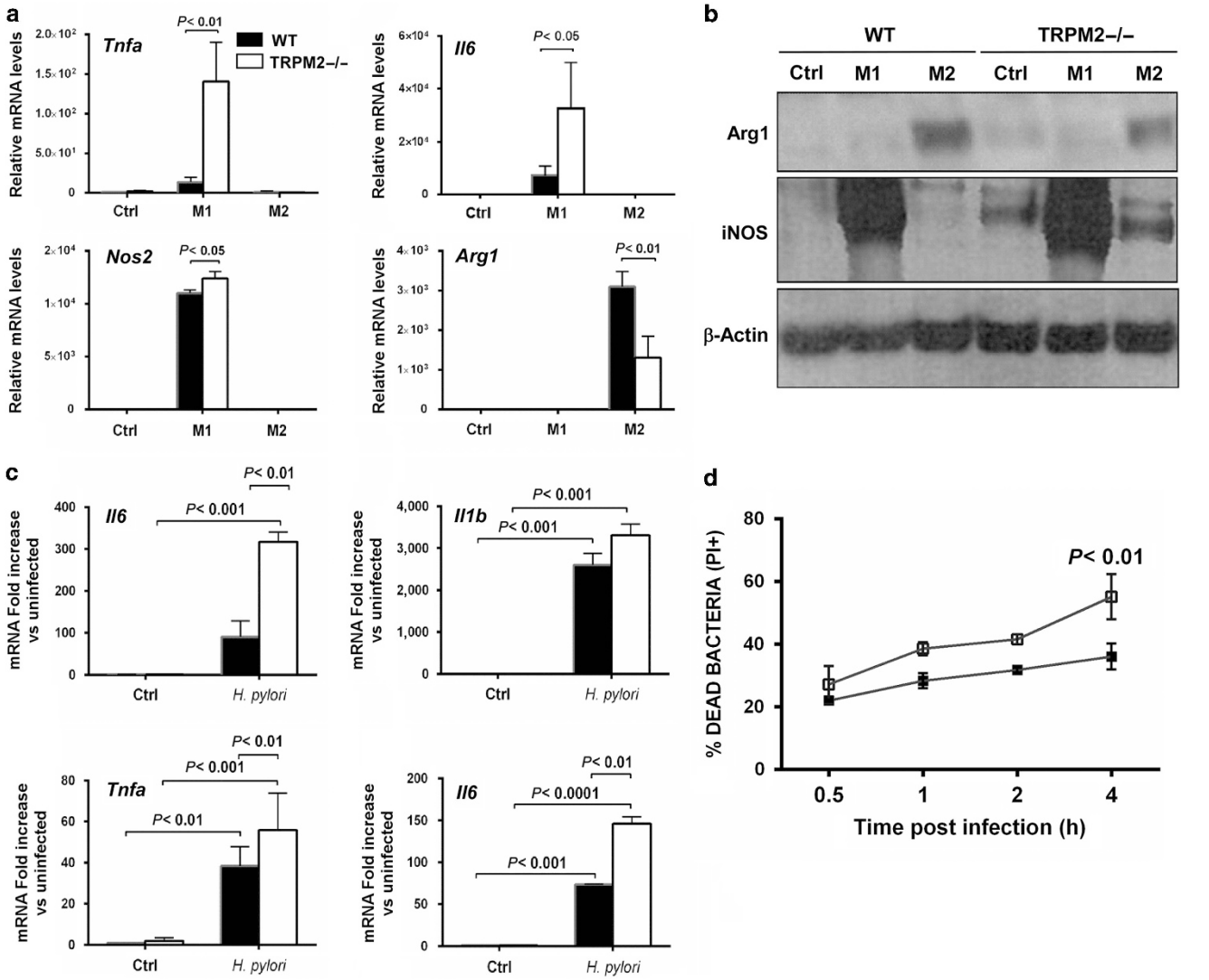

Figure 1 Transient receptor potential melastatin 2 (TRPM2) deficiency results in increased classical M1 polarization *in vitro* and *in vivo*. (**a**) Expression of genes associated with macrophage polarization in bone marrow-derived macrophage (BMDM) after 6 h of stimulation with M1-polarizing stimuli, lipopolysaccharide (LPS) (50 ng/ml) and interferon-γ (IFN-γ) (20 ng/ml), or M2-polarizing stimuli, interleukin-4 (IL-4) (20 ng/ml) and IL-13 (20 ng/ml). *Tnfa*, *il6*, *Nos2*, and *Arg1* expression levels were assessed by quantitative real-time PCR (qRT-PCR) and normalized to *Gapdh* levels. Data shown are representative of four independent experiments. (**b**) Arg1 and iNOS (inducible nitric oxide synthase) protein levels were assessed by western blotting after 24 h of M1-and M2-polarizing stimuli treatment of BMDM cells from wild-type (WT) and *Trpm2*$^{-/-}$ mice. A representative blot is shown. Similar results were observed in three independent experiments. (**c**) BMDMs from WT and *Trpm2*$^{-/-}$ mice were stimulated with *Helicobacter pylori* for 6 h, and RNA was isolated and subjected to qRT-PCR analysis of *Il12p40*, *Il1b*, *Tnfa*, and *Il6*. Expression was normalized to glyceraldehyde 3-phosphate dehydrogenase (GAPDH). The values shown are from four independent experiments. (**d**) Flow cytometry analysis of bactericidal activity. BMDMs from WT and *Trpm2*$^{-/-}$ mice were incubated with *H. pylori* (multiplicity of infection (MOI) of 10) for 1 h. Cells were then washed and further incubated for 0–4 h, and then lysed. The lysates were exposed to Syto 9 and propidium iodide (PI) to stain live and dead bacteria, respectively. Percentage of PI^{+} cells from 0.5 to 4 h after challenge is shown. (**c** and **d**) Data are representative of five independent experiments. Arg1, arginase 1; Ctrl, control.

enhanced bactericidal activity. Thus, we performed bactericidal killing assays in WT and TRPM2$^{-/-}$ BMDMs. After 4 h of coculture with *H. pylori*, TRPM2$^{-/-}$ BMDM had a significant increase in bacterial killing compared with WT BMDM (**Figure 1d**).

Chronically infected *Trpm2*$^{-/-}$ mice exhibit increased gastritis and decreased *H. pylori* colonization

The role of TRPM2 in regulating the immune response has been highly divergent depending on the model of inflammation evaluated. To determine the direct impact of TRPM2 on the chronic inflammatory process during *H. pylori*-induced gastric inflammation, WT and *Trpm2*$^{-/-}$ mice were orogastrically inoculated with *H. pylori* strain PMSS1. Histological examination of their stomach tissue at serial time points up to 6 months revealed that infection induced gastritis in both strains of mice, but *H. pylori*-infected *Trpm2*$^{-/-}$ mice had significantly more inflammation compared with *H. pylori*-infected WT mice at 1 month postinfection (**Figure 2a,b**).

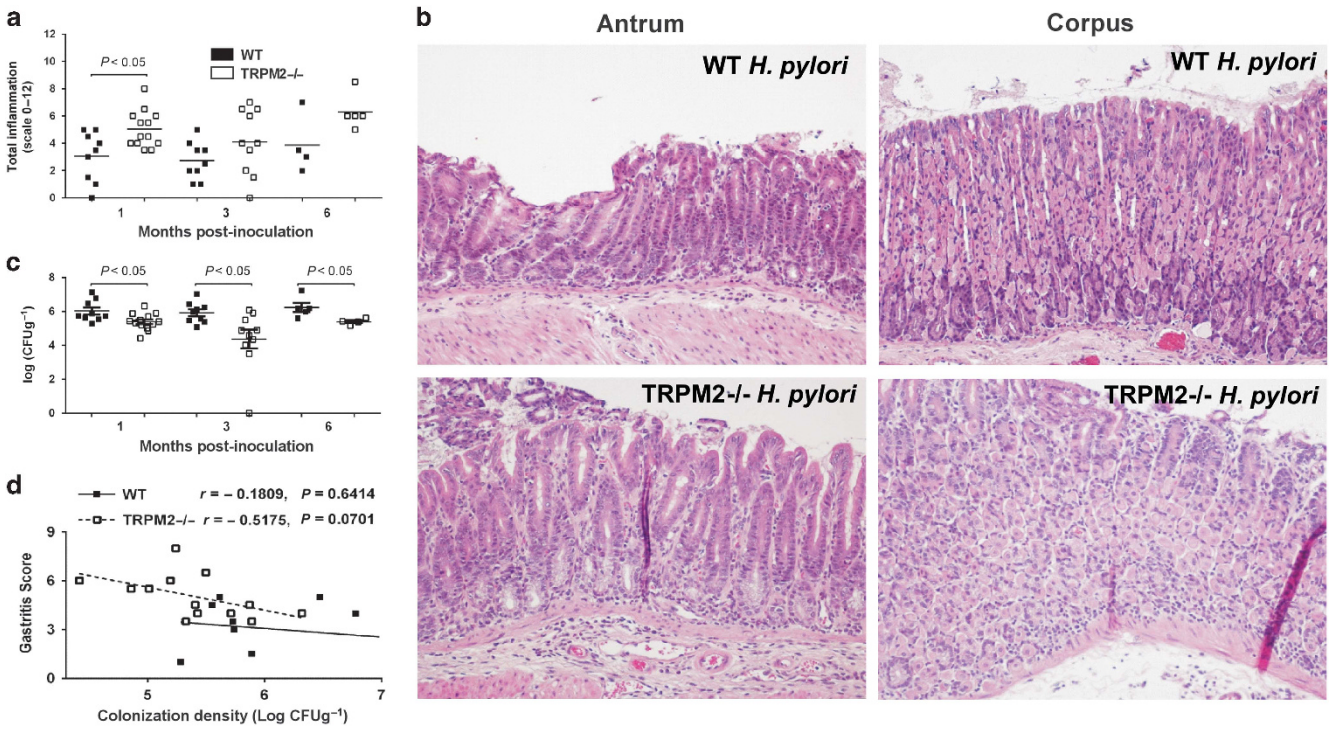

Figure 2 Lack of transient receptor potential melastatin 2 (TRPM2) improves control of *Helicobacter pylori* infection but aggravates gastric immunopathology (**a**) Gastric inflammation at 1, 3, and 6 months after *H. pylori* PMSS1 infection was assessed and scored (0–12) on stomach tissue (corpus and antrum) in wild-type (WT) and *Trpm2*$^{-/-}$ mice. Each data point represents inflammation scores from an individual animal. (**b**) Representative histologic images from *H. pylori*-infected WT antrum, *H. pylori*-infected WT corpus, *H. pylori*-infected TRPM2$^{-/-}$ antrum, and *H. pylori*-infected TRPM2$^{-/-}$ corpus mice at original magnification ×200. (**c**) Levels of colonization were measured by plating serial dilutions of stomach homogenates. The number of colony-forming unit (CFU) was then calibrated to the weight of the tissue and log CFU/g is presented on the graphs. (**d**) Colonization was plotted against total inflammation for each infected mouse. The lines illustrate the best-fit linear regressions obtained for the two strains of mice with the correlation coefficient and significance as indicated. Each point represents a single mouse. Similar results were also observed in two other independent experiments. Results from experiments with 4 to 13 mice per group and are representative of at least three independent experiments.

To determine if these changes in inflammation influenced control of the infection, *H. pylori* colonization levels were measured. *Trpm2*$^{-/-}$ mice exhibited significantly lower bacterial burden compared with WT mice at all times postinfection (**Figure 2c**). Notably, increased gastritis correlated significantly with decreased bacterial colonization in *Trpm2*$^{-/-}$ mice at 1 month postinfection, but there was no correlation in WT mice (**Figure 2d**). These data indicate that loss of TRPM2 results in more severe inflammation within the context of *H. pylori* infection and further suggests that the increased inflammation leads to reduced bacterial burden.

Loss of TRPM2 alters the gastric cytokine profile and iNOS production in *H. pylori*-infected mice

The increased gastritis in *H. pylori*-infected *Trpm2*$^{-/-}$ mice at 1 month post infection, a time point when inflammatory recruitment is also driven by the adaptive response, also correlated with significantly greater numbers of gastric F4/80^{+} macrophages compared with infected WT mice, as assessed by flow cytometry (**Figure 3a**) and immunofluorescence (**Supplementary Figure S2**).

TRPM2 was hypothesized to be an essential component in macrophage polarization during *H. pylori* infection *in vivo*. To test this, the expression of gene markers associated with M1- and M2-like polarization were assessed by qRT-PCR on positively selected F4/80^{+} macrophages from *H. pylori*-infected mice at 1month postinfection (**Figure 3b**). Gastric macrophages isolated from *H. pylori*-infected *Trpm2*$^{-/-}$ mice expressed significantly higher levels of M1-associated genes, *Il1b* and *Nos2*, compared with macrophages isolated from *H. pylori*-infected WT mice (**Figure 3b**). Immunofluorescence analysis on the antrum of infected animals revealed greater accumulation of F4/80^{+}/iNOS^{+}-infiltrating macrophages in the tissue of *Trpm2*$^{-/-}$ mice than in the WT mice (**Supplementary Figure S2a,b**). In contrast, expression of *Arg1* was significantly decreased in TRPM2$^{-/-}$ macrophages compared with WT macrophages (**Figure 3b**).

To investigate how innate and adaptive immune responses were affected by the loss of TRPM2 leading to increased inflammation in the gastric mucosa among *H. pylori*-infected mice, levels of the proinflammatory cytokines were measured (**Figure 3c**). Expression of *Il6* was significantly increased in the stomachs of infected *Trpm2*$^{-/-}$ mice at the 1 month time point. While quantification of *Il1b* revealed a trend toward increased expression of this cytokine in the *Trpm2*$^{-/-}$ mice at 3 months after the infection, as compared with infected WT mice, such differences did not reach statistical significance ($P = 0.0597$).

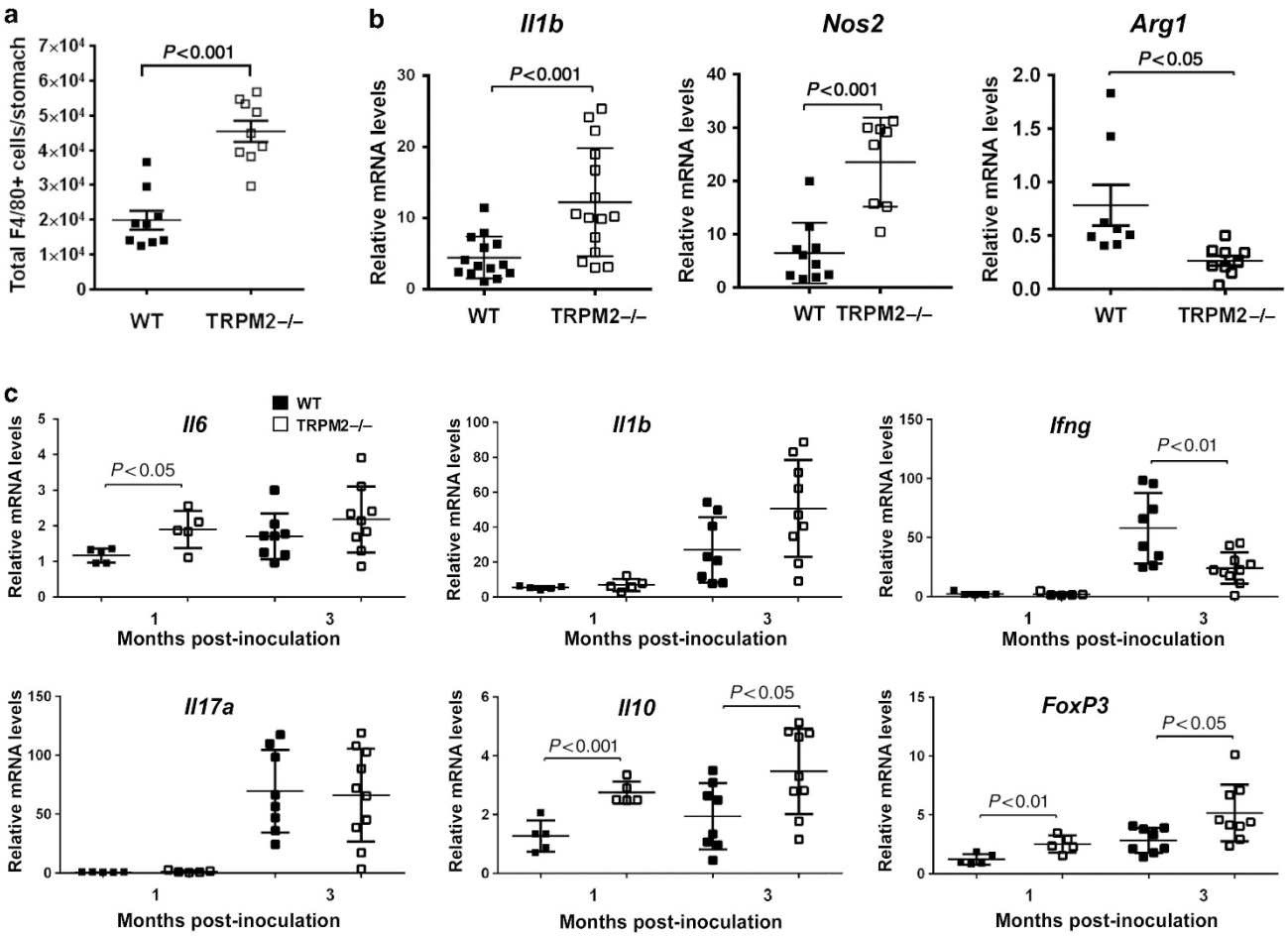

Figure 3 Innate, but not adaptive, inflammatory responses are increased in *Helicobacter pylori*-infected *Trpm2*$^{-/-}$ mice. Gastric cells were isolated from *H. pylori*-infected wild-type (WT) and Trpm2$^{-/-}$ mice killed at 1 month after challenge, and analyzed by flow cytometry for the expression of the macrophage marker F4/80. Total number of F4/80^{+} (gated on CD11b^{+} and Ly6C^{+}) cells per stomach is shown. (**a**) F4/80^{+} cells were isolated from the stomachs of WT and Trpm2$^{-/-}$ mice challenged with *H. pylori*, by magnet-assisted cell sorting (MACS). (**b**) RNA was isolated from macrophages and quantitative real-time PCR (qRT-PCR) was performed to analyze the expression of *Il1b*, *Nos2*, and *Arg1*. Expression was normalized to *Gapdh*. Each point represents data from an individual animal. Results shown are from experiments with 8 to 15 mice per group. Similar results were observed in two other independent experiments. WT and *Trpm2*$^{-/-}$ mice were infected with *H. pylori*. At 1 and 3 months postinfection, mice were killed, gastric tissues were removed, and RNA was extracted. (**c**) Relative mRNA levels of *Il6*, *Il1b*, and *Ifng* (top panel) or *Il17a*, *Il10*, and *Foxp3* (bottom panel) were measured by qRT-PCR. All qRT-PCR data were standardized to *Gapdh* mRNA. Relative mRNA levels of each point represent a single mouse. Results from experiments with 4 to 13 mice per group and are representative of at least three independent experiments. Gapdh, glyceraldehyde 3-phosphate dehydrogenase; TRPM, transient receptor potential melastatin 2.

On the other hand, increased innate proinflammatory cytokines did not translate to increased T-helper type 1 (Th1) or Th17 responses in the *Trpm2*$^{-/-}$ mice compared with WT mice. *Ifng* was significantly lower at 3 months postinfection in *H. pylori*-infected *Trpm2*$^{-/-}$ mice compared with *H. pylori*-infected WT mice. *H. pylori* infection elicits a mix of adaptive Th1, Th2, T-regulatory cells (Tregs), and Th17 responses in the gastric mucosa.[23] Consistent with a previous report,[24] the levels of *Il17a* were increased in all *H. pylori*-infected mice, but there were no differences between the WT and *Trpm2*$^{-/-}$ mice. Interestingly, *Il10* and the transcriptional regulator of Tregs, *Foxp3*, were expressed at significantly higher levels in *Trpm2*$^{-/-}$ mice compared with WT mice at 1 and 3 months after infection. Taken together, these data suggest that the exacerbated inflammatory response observed in *H. pylori*-infected *Trpm2*$^{-/-}$ mice is likely a result of hyperinflammatory innate immune cell activity rather than proinflammatory Th1 or Th17 cytokines. Moreover, increased activation of macrophages and ROS production may drive a stronger Treg response in the TRPM2$^{-/-}$ mice during *H. pylori* infection.

TRPM2 protects against excessive NADPH-oxidase activity and ROS production in *H. pylori* infection

The TRPM2 channel's function in macrophages is linked to NADPH activity, ROS production, and subsequent cytokine and chemokine expression.[7,9–11] Moreover, as ROS production is known to be involved in the development of gastric inflammation during *H. pylori* infection,[25] we sought to define whether chronic *H. pylori* infection leads to changes in components of the oxidative burst pathway. Significantly greater levels of NADPH-oxidase 2 (*Nox2*/gp91phox/CYBB)

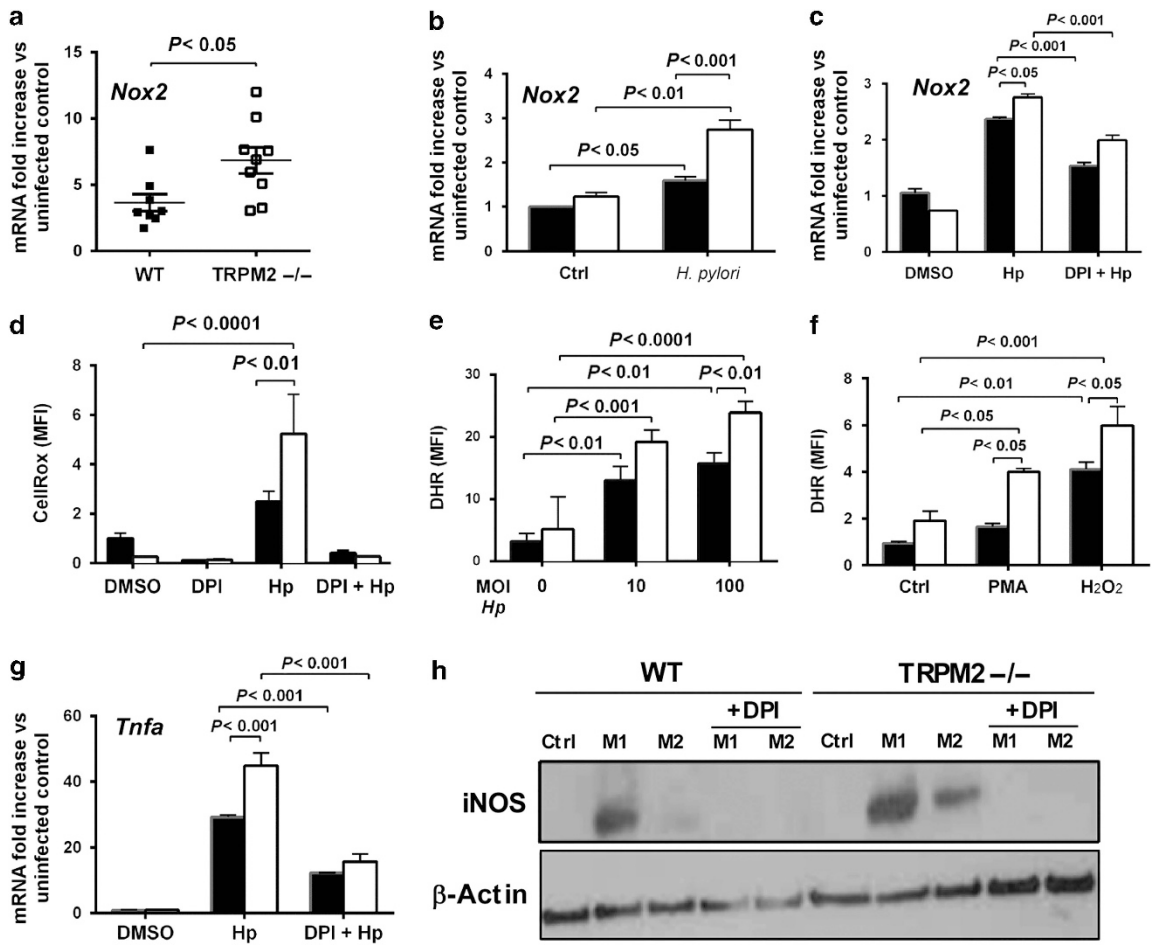

Figure 4 Transient receptor potential melastatin 2 (TRPM2) deficiency promotes nicotinamide adenine dinucleotide phosphate (NADPH)-oxidase activity and oxidative stress during infection with *Helicobacter pylori*. (**a**) *Nox2* mRNA levels were measured by quantitative real-time PCR (qRT-PCR) from the stomach of *H. pylori*-infected WT and *Trpm2*$^{-/-}$ mice killed at 3 months after challenge. Data were standardized to *Gapdh*. Each point represents a single mouse. (**b**) *Nox2* transcript abundance in wild-type (WT) and TRPM2$^{-/-}$ bone marrow-derived macrophage (BMDM) was determined by qRT-PCR, and values were normalized with respect to *Gapdh* mRNA. (**c**) qRT-PCR analysis of *Nox2* mRNA levels from WT and TRPM2 BMDM stimulated with *H. pylori*, and pretreated with diphenyleneiodonium (DPI) when indicated. Values were normalized with respect to *Gapdh* mRNA. (**d**) Release of ROS, assessed as CellROX fluorescence in WT and TRPM2$^{-/-}$ BMDM left unstimulated (dimethyl sulfoxide (DMSO)) or stimulated with *H. pylori* (multiplicity of infection (MOI) of 50), or additional pretreatment with DPI (10 μM), presented as relative fluorescence. (**e**) Hydrogen peroxide (H_2O_2) release measured by dihydro-rhodamine 123 (DHR123) oxidation in controls and *H. pylori*-stimulated WT and TRPM2$^{-/-}$ BMDM, presented as relative fluorescence. (**f**) Assessment of H_2O_2 release by DHR123 fluorescence in WT and TRPM2$^{-/-}$ BMDM left unstimulated (Control), or stimulated with phorbol 12-myristate 13-acetate (PMA) (1 μM) or H_2O_2 (10 μM), presented as relative fluorescence. (**g**) WT and TRPM2$^{-/-}$ BMDM were infected with *H. pylori*, with or without pretreatment with DPI (10 μM), and expression of *Tnfa* was examined by qRT-PCR analysis. (**b**–**g**) The values shown are from four independent experiments. (**h**) WT and TRPM2$^{-/-}$ BMDMs were infected with *H. pylori*, with or without pretreatment with DPI (10 μM), and protein level of inducible nitric oxide synthase (iNOS) was examined by western blot analysis. Data were standardized to β-actin. Western blots are representative of three independent experiments with similar results. Gapdh, glyceraldehyde 3-phosphate dehydrogenase.

mRNA were detected in *H. pylori*-infected *Trpm2*$^{-/-}$ mice compared with *H. pylori*-infected WT mice at 3 months postinfection (**Figure 4a**). Similarly, when cultured with *H. pylori*, TRPM2$^{-/-}$ BMDM had significantly higher expression of *Nox2* mRNA compared with WT BMDM (**Figure 4b**). To test the hypothesis that macrophages from *Trpm2*$^{-/-}$ mice might also exhibit increased ROS production in response to *H. pylori*, ROS production was measured in BMDM cocultured with *H. pylori* using CellROX (Thermo Fisher Scientific, Carlsbad, CA). We observed significantly increased ROS generation in TRPM2$^{-/-}$ macrophages cocultured with *H. pylori* compared with WT macrophages (**Figure 4d**). Similarly, *H. pylori*-infected or phorbol 12-myristate 13-acetate-stimulated TRPM2$^{-/-}$ macrophages have significantly higher intracellular H_2O_2 levels (**Figure 4e,f**). Conversely, pretreatment with diphenyleneiodonium (DPI), an NADPH-oxidase inhibitor,[26] abrogated the enhanced ROS production and *Nox2* expression in TRPM2$^{-/-}$ and WT macrophage cocultures with *H. pylori* (**Figure 4c,d**).

As augmented ROS production has been correlated to increases in proinflammatory cytokine production,[27,28] we measured the gene expression of *Tnfa* in BMDM stimulated with *H. pylori* in the presence or absence of DPI treatment. Pretreatment with DPI diminished the expression of *H. pylori*-induced *Tnfa* in both TRPM2$^{-/-}$ and WT BMDMs (**Figure 4g**), indicating that the increase in *Tnfa* in the

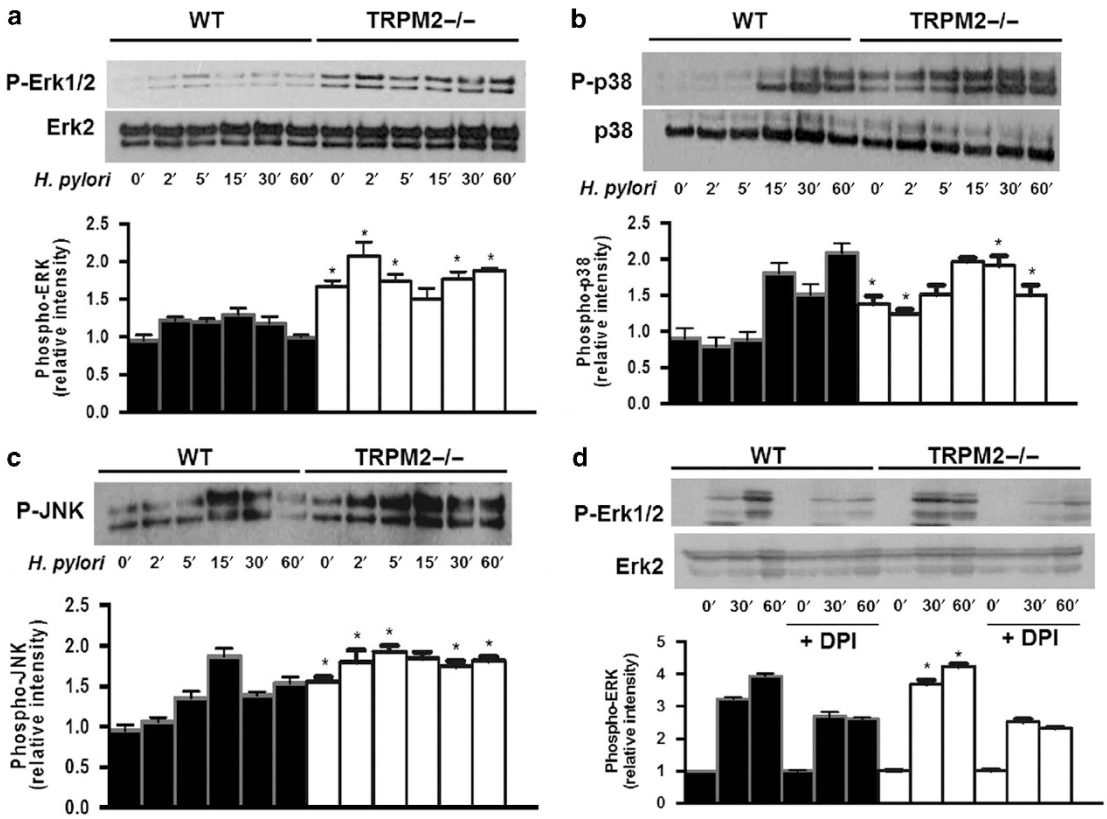

Figure 5 Transient receptor potential melastatin 2 (TRPM2) ablation augments *Helicobacter pylori*-induced mitogen-activated protein kinase (MAPK) activation. Bone marrow-derived macrophages (BMDMs) from wild-type (WT) and *Trpm2*$^{-/-}$ mice were cocultured with *H. pylori* (multiplicity of infection (MOI) of 10) for the indicated time points, and activity of extracellular signal-regulated protein kinase (ERK) (**a**), p38 (**b**), and c-Jun N-terminal kinase (JNK) (**c**) were examined by western blot analysis using phosphospecific antibodies. The total protein levels of ERK and p38 were also measured. (**d**) WT and TRPM2$^{-/-}$ BMDMs were pretreated with dimethyl sulfoxide (DMSO) or diphenyleneiodonium (DPI) (10 μM) before stimulation with *H. pylori* at the indicated times. The phosphorylation of ERK1/2 was analyzed by western blot. (**a**–**d**) Densitometric analysis for each MAPK band is displayed beneath western blot, respectively. Western blots shown are representative of three independent experiments with similar results. Statistical analyses are performed comparing differences between WT and TRPM2$^{-/-}$ cells at each time point (*$P<0.05$).

TRPM2$^{-/-}$ macrophages is dependent on ROS production. Moreover, in the presence of DPI, protein levels of iNOS were significantly reduced in M1- and M2-polarized TRPM2$^{-/-}$ BMDM and WT BMDM (**Figure 4h**). These results suggest that TRPM2-dependent signaling may be an important downregulating expression of proinflammatory mediators and therefore important for reducing gastric damage during *H. pylori* infection through NADPH-oxidase-mediated ROS downregulation.

TRPM2 negatively regulates *H. pylori* induced ERK, JNK, and p38 activation

In addition to the abundant evidence for activation of elements of the MAPK system by NADPH oxidases,[29,30] *H. pylori* has been reported to activate the MAPK superfamily.[31–33] Thus, we hypothesized that exacerbated TRPM2$^{-/-}$ macrophage inflammatory responses may result in enhanced MAPK signaling in response to *H. pylori*. Indeed, coculture of BMDM with *H. pylori* increased extracellular signal-regulated protein kinase 1/2 (ERK1/2), p38, and c-Jun N-terminal kinase (JNK) activation in WT and TRPM2$^{-/-}$ BMDMs (**Figure 5a,c**). Unlike WT BMDM, TRPM2$^{-/-}$ BMDM demonstrate constitutive ERK, p38, and JNK phosphorylation, which was enhanced and prolonged after coculture with *H. pylori* compared with WT macrophages (**Figure 5a,c**). Quantitative densitometry demonstrated a marked increase in phosphorylation of MAPKs in TRPM2$^{-/-}$ BMDM compared with WT BMDM (**Figure 5a–c**). DPI treatment decreased the phosphorylation level of ERK1/2 induced by *H. pylori* at selected time points in WT and TRPM2$^{-/-}$ BMDMs (**Figure 5d**), suggesting that the altered MAPK signaling observed in TRPM2$^{-/-}$ BMDM is dependent on NADPH activity and ROS production.

H. pylori-activated TRPM2 channels are required for intracellular Ca^{2+} homeostasis in macrophages

To establish the functional link between TRPM2 and the Ca^{2+} responses orchestrated by *H. pylori* infection in macrophages, we first assessed the presence of the TRPM2 channel in response to *H. pylori* stimulation in these cells. As reported previously,[10] we confirmed that the channel is constitutively expressed in mouse macrophages. Furthermore, we observed that only M2 polarization of macrophages increased TRPM2 transcripts levels compared with M1 or *H. pylori*-infected

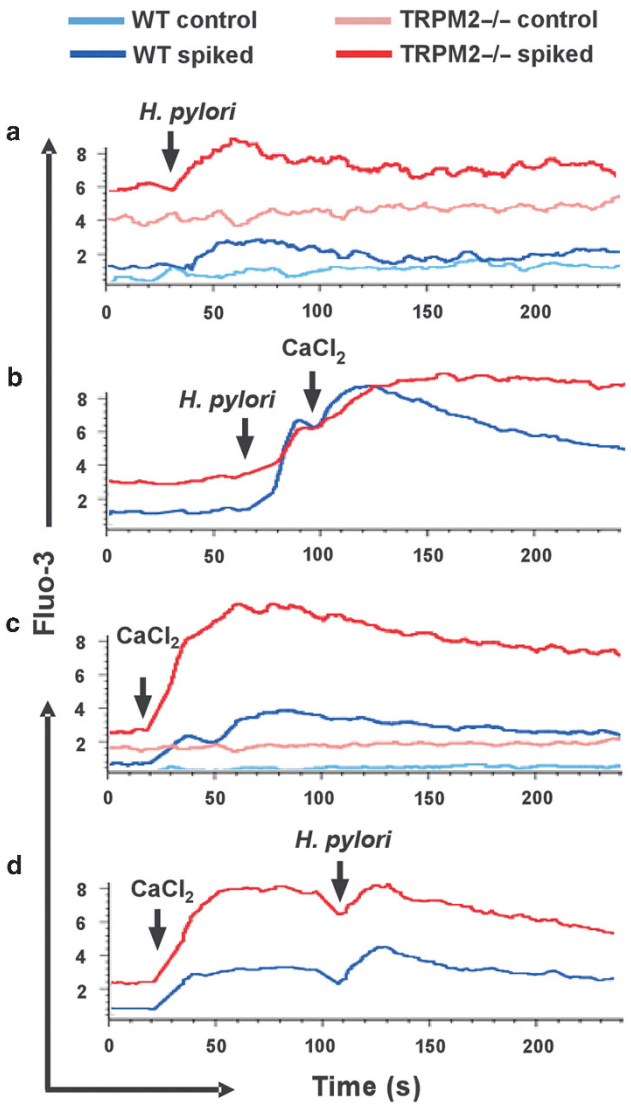

Figure 6 *Helicobacter pylori* modulates intracellular Ca^{2+} levels in macrophages. Free intracellular Ca^{2+} levels were measured by flow cytometry in wild-type (WT) and TRPM2$^{-/-}$ bone marrow-derived macrophage (BMDM) loaded with the fluorescent Ca^{2+} indicator Fluo-3. Cells were spiked with (**a**) *H. pylori* (multiplicity of infection (MOI) of 100), (**b**) *H. pylori* followed by $CaCl_2$ (2 mM), (**c**) $CaCl_2$ (2 mM), or (**d**) $CaCl_2$ (2 mM) followed by *H. pylori* at the indicated time. Accumulation of free Ca^{2+} was measured by flow cytometry over the next 4 min. One of three independent experiments is shown. TRPM2, transient receptor potential melastatin 2.

macrophages (**Supplementary Figure S3a**). This TRPM2 expression pattern was also observed in human M2 macrophages (**Supplementary Figure S3b**), suggesting that enhanced TRPM2 expression might favor anti-inflammatory phenotype in macrophages.

Because TRPM2 is involved in the modulation of Ca^{2+} homeostasis, we sought to determine the specific contribution of the channel by measuring the intracellular Ca^{2+} concentration ($[Ca^{2+}]_i$) in *H. pylori*-stimulated WT and TRPM2$^{-/-}$ macrophages. *H. pylori* triggered a small, but detectable increase in $[Ca^{2+}]_i$, which rapidly declined to baseline levels in both WT and TRPM2$^{-/-}$ macrophages, as indicated by increased fluorescence of the Ca^{2+} indicator Fluo-3AM (**Figure 6a**). This Ca^{2+} signal represents release of Ca^{2+} from intracellular stores, as these experiments are performed in Ca^{2+}-free medium. Importantly, TRPM2$^{-/-}$ macrophages showed an increase in both baseline and *H. pylori*-stimulated responses, as indicated by the higher relative fluorescence. Addition of extracellular Ca^{2+} resulted in higher Ca^{2+} entry from the plasma membrane, which gradually declined over the next 4 min in *H. pylori*-stimulated WT BMDM (**Figure 6b**, blue trace). In contrast, in TRPM2$^{-/-}$ BMDM (red trace), Ca^{2+} entry was increased at a slower rate, and $[Ca^{2+}]_i$ remained elevated for at least 4 min after *H. pylori* stimulation. Similar results were observed when macrophages were maintained under Ca^{2+}-free conditions and then spiked with $CaCl_2$ (2 mM) (**Figure 6c**) only, or with $CaCl_2$ (2 mM) followed by *H. pylori* (**Figure 6d**) at the indicated times.

These data suggest that lack of functional TRPM2 channels in macrophages leads to Ca^{2+} dysregulation and subsequent increases in $[Ca^{2+}]_i$ following *H. pylori* infection may be one of the mechanisms by which Ca^{2+}-dependent macrophage functions are being affected in TRPM2$^{-/-}$ macrophages.

To investigate the activity of the TRPM2 channel in the plasma membrane of macrophages upon *H. pylori* infection, we measured whole-cell currents in WT and TRPM2$^{-/-}$ macrophages using patch-clamp electrophysiology. First, current activation induced by intracellular perfusion of 200 μM ADPR, the specific agonist of TRPM2, showed a linear current–voltage (*I–V*) relationships with a reversal potential and around 0 mV, which is characteristic for TRPM2 (**Figure 7a**).[6] Because *H. pylori* stimulation induced intracellular Ca^{2+} release followed by robust plasma membrane Ca^{2+} entry as in **Figure 6b**, we reasoned that *H. pylori* might trigger extracellular Ca^{2+} uptake via TRPM2 and/or additional plasma membrane channels. To test the participation of TRPM2 in Ca^{2+} entry mediated by *H. pylori* stimulation, voltage-clamped macrophages derived from WT or *Trpm2*$^{-/-}$ mice were perfused with a solution containing *H. pylori*. Interestingly, the application of solution containing *H. pylori* evoked currents that were higher in amplitude compared with ADPR-induced WT macrophages, but resembled the characteristic *I–V* relationship of TRPM2[6] (**Figure 7b,d**). Stimulation of TRPM2$^{-/-}$ macrophages with *H. pylori* induced minimal development of whole-cell currents compared with WT macrophages (**Figure 7b**). The data suggest that TRPM2-mediated currents contribute significantly to *H. pylori*-induced current activation, and likely impact downstream regulation of Ca^{2+}-dependent macrophage functions.

H_2O_2, which is known to increase intracellular ADP-ribose formation, can be generated through activation of the NADPH oxidase. To confirm whether *H. pylori*-induced NADPH oxidase might subsequently result in opening of TRPM2 channels, we tested the effects of DPI on TRPM2 current development by whole-cell patch-clamp electrophysiology. When WT macrophages were perfused with *H. pylori*, TRPM2 currents developed to an average peak current of ~20 pA pF^{-1}, over a range of time between 0 and 700 s

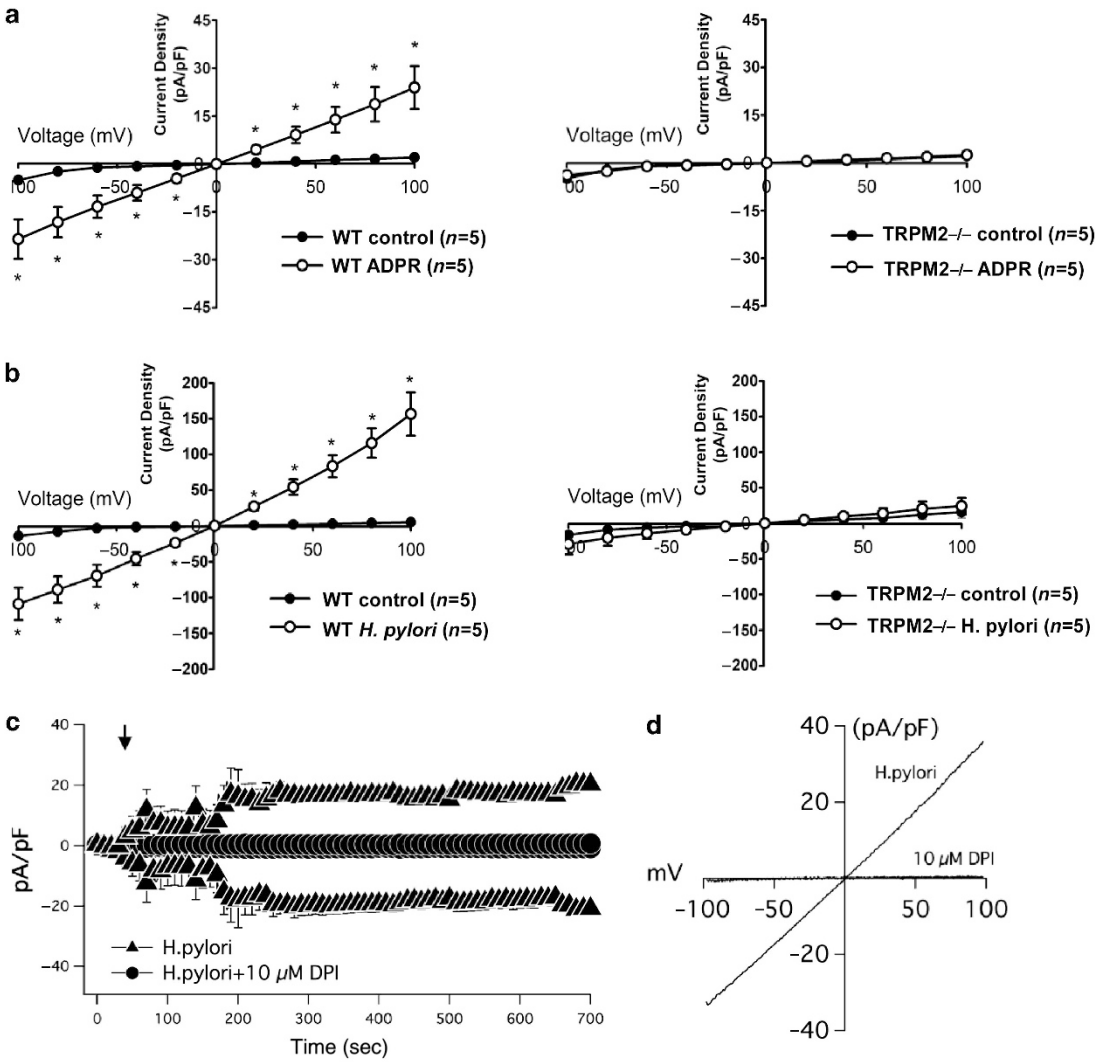

Figure 7 *Helicobacter pylori* modulates membrane conductance of macrophages through transient receptor potential melastatin 2 (TRPM2). (**a**) Current–voltage (*I–V*) relationship of *H. pylori*-induced membrane conductance in wild-type (WT) and TRPM2$^{-/-}$ cells. Current traces of (left panel) WT or (right panel) TRPM2$^{-/-}$ bone marrow-derived macrophage (BMDM) by voltage-clamp recording when perfused with control, (**a**) adenosine diphosphate ribose (ADPR) (200 μM) or (**b**) *H. pylori* suspension at 1×10^6 CFU/ml. (**c**) BMDMs were suspended in Hank's buffer with (circles) or without (triangles) diphenyleneiodonium (DPI) (10 μM), and then electrophysiological measurements were recorded in whole-cell configuration for temporal development of inward and outward currents in WT cells by voltage-clamp recordings when cells were perfused with *H. pylori* containing buffer. (**d**) *I–V* relationship of *H. pylori* alone (*H. pylori*), and *H. pylori* in WT cells preincubated with 10 μM DPI. Data are expressed as mean ± s.e.m., $n = 7$–20.

(**Figure 7c**). Interestingly, DPI-pretreated cells failed to develop TRPM2 currents after the application of *H. pylori* (**Figure 7c,d**). The *I–V* relationship was characteristic of TRPM2 channels (**Figure 7d**), and DPI-pretreated cells showed little to no inward or outward currents (**Figure 7d**), suggesting that NADPH-oxidase activity and H_2O_2 production in response to *H. pylori* are required for the activation of TRPM2-dependent signaling.

To test the hypothesis that Ca^{2+} overloading observed in *H. pylori*-stimulated TRPM2$^{-/-}$ macrophages is mediated through another ion channel at the plasma membrane, we investigated the expression and function of TRPM7 in BMDM. Previous studies have shown that TRPM7 has a role in regulating ROS, nitric oxide production, and inflammation.[34–36] To examine TRPM7 regulation in TRPM2$^{-/-}$ and WT macrophages, we first evaluated TRPM7 protein expression in BMDM. Western blotting for TRPM7 protein expression on cell lysates indicated that TRPM7 expression was modestly upregulated in TRPM2$^{-/-}$ macrophages compared with WT macrophages (**Supplementary Figure S4a**). Nevertheless, electrophysiological patch-clamp measurements demonstrate that TRPM7 currents were significantly increased in TRPM2$^{-/-}$ macrophages ($n = 10$) compared with WT macrophages ($n = 12$). Peak TRPM7 currents were ~25 and ~12 pA pF^{-1} in TRPM2$^{-/-}$ and WT macrophages, respectively (**Supplementary Figure S4b**). The *I–V* relationship was characteristic of TRPM7, displaying an outwardly rectified current and very little inward current (**Supplementary Figure S4c**). These results suggest TRPM7 channel activity is increased in the absence of TRPM2, and may contribute to the Ca^{2+} overloading in these cells. In conclusion, our hypothetical

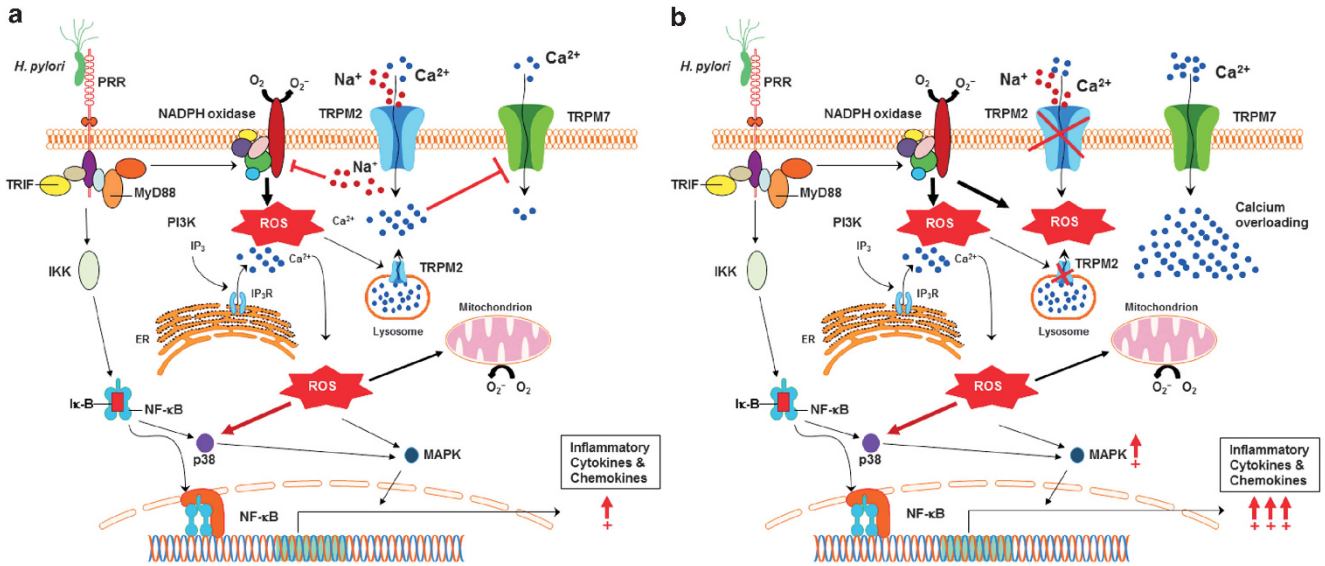

Figure 8 Model of transient receptor potential melastatin 2 (TRPM2)-mediated signaling mechanisms in macrophages during *Helicobacter pylori* infection. (**a**) *H. pylori* engages pattern of recognition receptors (PRRs), e.g., toll-like receptors (TLRs), which recruit MyD88 and TRIF adaptor proteins that may trigger the activation of phosphatidylinositol 3-kinase (PI3K), followed by an increase of intracellular concentration of Ca^{2+} via release of inositol-1,4,5-trisphosphate Ins(1,4,5)P_3R channel located on the endoplasmic reticulum (ER) or putative expression of lysosomal TRPM2 channel, respectively. The rise in the cytosolic Ca^{2+} concentration and the activity of PI3K lead to the activation of mitogen-activated kinases (MAPKs) and other kinases that phosphorylate the cytosolic subunits of the nicotinamide adenine dinucleotide phosphate (NADPH) oxidase of phagocytes, activating their migration to the plasma membrane and enhancing production of reactive oxygen species (ROS). Increased ROS contributes to increased inflammatory gene expression through Ca^{2+}-dependent signaling pathways, such as MAPK and nuclear factor-κB (NF-κB) transcription factors. Oxidants, including H_2O_2, may mobilize adenosine diphosphate ribose (ADPR) from mitochondria (both H_2O_2 and Ca^{2+} can synergize with ADPR to activate TRPM2) stimulating additional cation entry across plasma membrane TRPM2. Intracellular accumulation of Na^+ through TRPM2 mediates membrane depolarization, which inhibits NADPH-oxidase activity, then limiting the inflammatory cascade. (**b**) In the absence of TRPM2, the initial PI3K-dependent, IP_3-mediated spike of cytosolic Ca^{2+} will rapidly return to baseline levels. Moreover, NADPH-oxidase activity will not be restricted, resulting in further increment in ROS accumulation and consequently dysregulated enhancement of inflammatory signaling pathways. Persistent cell stimulation by *H. pylori* in the TRPM2 knockout will result in transitory Ca^{2+} starvation that may be the driving force for the opening of additional cation channels at the plasma membrane (e.g., TRPM7), which will enable compensatory mechanisms of Ca^{2+} entry favoring cytosolic Ca^{2+} overload, and hence the extension of exacerbated inflammatory signals.

working model (**Figure 8**) indicates that *H. pylori* stimulation induces strong NADPH-oxidase function and consequently TRPM2 activation, which in turn limits NADPH-oxidase activity and prevents excessive inflammation (**Figure 8a**). In contrast, Ca^{2+} overloading in the TRPM2-deficient macrophages favors polarization toward the proinflammatory M1 phenotype and concomitantly this activity enhances oxidative stress through unregulated NADPH-oxidase activity, followed by increased generation of intracellular ROS. Taken together, our data support the hypothesis that TRPM2 channels work as a functional cellular rheostat that controls ion currents at the plasma membrane, thereby regulating Ca^{2+} homeostasis and macrophage oxidative functions during *H. pylori* infection.

DISCUSSION

Regulation of intracellular Ca^{2+} concentration is a tightly controlled process. However, the molecular players involved in shaping intracellular Ca^{2+} signals are poorly characterized in phagocytes. The current paradigm states that increases in cytosolic Ca^{2+} levels are caused by activation of cell surface receptor by endogenous or exogenous stimuli, which trigger the release of Ca^{2+} from endoplasmic reticulum Ca^{2+} stores, and is followed by Ca^{2+} entry through the plasma membrane via Ca^{2+} release-activated Ca^{2+} current channels.[37–39] However, macrophages express a variety of additional ion channels including the TRP channels, which have recently emerged as essential regulators of important physiological functions in macrophages.[4,5] In addition to conducting ions through the plasma membrane, some TRP channels may also function to couple endoplasmic reticulum-to-plasma membrane signaling crosstalk or to release Ca^{2+} from internal stores contributing to global cellular Ca^{2+} homeostasis.[5,40] Specific members of the TRPM and TRPC subfamilies have been associated with Ca^{2+} mobilization functions in phagocytic cells including chemotaxis, phagocytosis, and cytokine secretion.[41,42]

We previously reported that TRPM2, a nonselective Ca^{2+}-permeable channel abundantly expressed in phagocytic cells, has essential roles in chemotaxis of polymorphonuclear leukocytes, macrophages, and dendritic cells,[14,43] and during activation and maturation of dendritic cells.[14] Because TRPM2 has been extensively proposed as an oxidative stress sensor and *H. pylori* infection causes oxidative stress in the gastric mucosa, we addressed the function of TRPM2 in macrophages using *H. pylori* infection as our chronic inflammation model. Our findings show that the loss of TRPM2 results in increased *H. pylori*-induced gastritis and decreased bacterial colonization in mice. Indeed, gastritis inversely correlated with bacterial colonization density in the *Trpm2*$^{-/-}$ mice. These data also

support the finding that TRPM2$^{-/-}$ macrophages demonstrated increased bacterial killing activity and augmented the levels of proinflammatory cytokines compared with WT macrophages, indicating TRPM2 has a regulatory and anti-inflammatory function.

Although other research groups had previously attempted to elucidate the effects of TRPM2 in distinct models of inflammation or infection,[8,11,44,45] these studies have yielded conflicting results. Yamamoto *et al.*[8] reported the first TRPM2-deficient mouse model. The initial studies showed that ROS-dependent activation of TRPM2 was crucial for chemokine production in mouse monocytes. Moreover, ROS-induced Ca^{2+} influx through TRPM2 triggered Ca^{2+}-dependent tyrosine kinase Pyk2 and Erk signaling, and thus led to the inflammatory nuclear translocation of nuclear factor-κB. Monocytes of *Trpm2*$^{-/-}$ mice also displayed a reduced production of the chemokine CXCL2, homolog to human CXCL8. Interestingly, *Trpm2*$^{-/-}$ mice upon dextran sulfate sodium-induced colitis exhibited reduced release of IFN-γ and IL-12 cytokines. In addition, in this dextran sulfate sodium model, neutrophil infiltration and ulceration were attenuated in *Trpm2*$^{-/-}$ mice compared with WT mice, suggesting that TRPM2 may aggravate inflammation. Another study supporting a proinflammatory role for TRPM2 demonstrated that TRPM2 function and Ca^{2+} entry were also required for LPS-induced production of IL-6, TNF-α (tumor necrosis factor-α), IL-8, and IL-10 in human monocytes.[46] These data shed little light on the mechanism by which TRPM2 positively regulates secretion of inflammatory cytokines in response to dextran sulfate sodium or LPS. In both cases, however, increased intracellular levels of Ca^{2+} appeared to have a critical role in activating such cytokine secretion. More recently, another TRPM2-deficient mouse was generated by GlaxoSmithKline (GSK, Brentford, London, UK). The first report using these animals showed that the absence of TRPM2 exacerbated inflammation in the lungs of mice systemically exposed to LPS. In addition, authors also found increased amounts of the proinflammatory cytokines CXCL2, TNF-α, and IL-6 in the lungs of *Trpm2*$^{-/-}$ mice.[11] Furthermore, NADPH-oxidase-mediated production of ROS was greater in the lungs and BMDM isolated from *Trpm2*$^{-/-}$ as compared with WT mice. They proposed that TRPM2 inhibits ROS production in macrophages through TRPM2-induced plasma membrane depolarization dampening the NADPH-oxidase activity.[11] While the chronic elevation of ROS in the *H. pylori* model presented here could contribute to gastritis and tissue damage, it may also explain the increased level of Tregs and therefore the reduction in Th1 responses. It has been demonstrated that Tregs are hyperfunctional in elevated levels of ROS,[47,48] and therefore oxidative stress may actually trigger Tregs, which are poised to suppress the excessive inflammation in the TRPM2-knockout mice.

Although LPS is widely accepted as a model of endotoxin-mediated inflammation, differences in routes of LPS administration, doses, and experimental readouts limit the reproducibility of the model and do not mimic the natural response to an infection. Therefore, we turned to a chronic persistent bacterial infection model to investigate how TRPM2 affects inflammation and oxidative stress responses. Our data demonstrate that TRPM2$^{-/-}$ macrophages exhibit strong functional M1 polarization characterized by increased production of iNOS and enhanced NADPH-oxidase activity via upregulation of NOX2, which resulted in greater accumulation of ROS. Positive regulation of NADPH oxidase correlated with an early and prolonged phosphorylation of MAPK ERK, p38, and JNK in response to *H. pylori* in TRPM2$^{-/-}$ as compared with WT macrophage responses. Despite the fact that we have used *Trpm2*$^{-/-}$ mice reported by Yamamoto *et al.*[8] in our studies, data are in good agreement with findings on *Trpm2*$^{-/-}$ mice from GSK, wherein TRPM2 activation downregulates macrophage inflammatory functions by restricting NADPH-oxidase function. However, Perraud and co-workers,[44] using GSK animals, reported increased morbidity and mortality in *Trpm2*$^{-/-}$ mice upon intravenous injection of *L. monocytogenes*. Although suppressed production of IFN-γ, IL-12, and iNOS were correlated with increased bacterial burden and greater *Trpm2*$^{-/-}$ mice mortality, septicemia was not evaluated as the possible cause of death in *L. monocytogenes*-infected *Trpm2*$^{-/-}$ mice.[44] Clearly, the origin of the *Trpm2*$^{-/-}$ mouse models available may not be the only condition to consider for the experimental discrepancies observed.

Previously published data suggest that TRPM2 facilitates plasma membrane depolarization[11] and this poses a potential explanation of how TRPM2 deficiency leads to increased NADPH oxidase and enhanced ROS production in our model. An additional mechanism, which can further explain enhanced oxidative responses in the absence of TRPM2, is the disruption of Ca^{2+} homeostasis in phagocytes. Indeed, increases in $[Ca^{2+}]_i$ levels and the activation of Ca^{2+}-dependent protein kinase C and its downstream MAPK have been directly associated with induction of NADPH-oxidase activity.[49] We surmised that TRPM2-mediated membrane depolarization is a transient event that may not fully account for the chronic inflammatory state of the macrophages, or the strong M1 polarization and resistance to M2 conversion observed in TRPM2$^{-/-}$ macrophages. As uptake of Na^+ via TRPM2 results in membrane depolarization, and thereby reduces Ca^{2+} entry, we reasoned that TRPM2$^{-/-}$ cells lacking this regulatory pathway upon stimulation may undergo transitory Ca^{2+} starvation, and therefore be prone to Ca^{2+} overloading and consequently altered Ca^{2+} homeostasis (hypothetical model depicted in **Figure 8**). As predicted, at baseline, TRPM2$^{-/-}$ macrophages exhibited slightly increased intracellular Ca^{2+} levels, ROS production, and MAPK phosphorylation. Strikingly, addition of *H. pylori* induced a moderate transient spike of Ca^{2+} release followed by large and prolonged influx of Ca^{2+}, resulting in a significant increase in intracellular Ca^{2+} levels in the TRPM2$^{-/-}$ macrophages, whereas Ca^{2+} influx in the WT cells returned to baseline levels after few minutes. Taken together, these data suggest that TRPM2 mediates membrane currents and Ca^{2+} homeostasis

in macrophages and thereby regulates NADPH activity. Similar to TRPM2, another member of the TRPM subfamily, TRPM4, was reported to perform Ca^{2+} regulatory function in dendritic cells.[50] Notably, bacterial stimulation, but not LPS, induced Ca^{2+} overloading in TRPM4$^{-/-}$ dendritic cells [50]. Similarly, we observed changes in intracellular Ca^{2+} levels and TRPM2 developed currents by electrophysiological patch-clamp measurements when the cells were stimulated with *H. pylori*. These data highlight the idea that bacterial, as opposed to endotoxin-induced, stimulation of macrophages recapitulates better the signaling pathway during natural infection and inflammation.

The molecular mechanism by which extracellular Ca^{2+} entry activates NADPH-oxidase activity is not completely understood; however, several published studies have provided evidence for the requirement of extracellular Ca^{2+} entry for NADPH-oxidase activation.[51–53] The link between Ca^{2+} entry and NADPH-oxidase activation is further supported by a significant decrease of superoxide anion production when extracellular Ca^{2+} is suppressed or chelated by EGTA.[53] Additional plasma membrane channels that conduct the required Ca^{2+} signal enhancing NADPH oxidase may contribute to Ca^{2+} overloading in TRPM2$^{-/-}$ macrophages. An additional member of the TRPM subfamily, TRPM7, is expressed at the plasma membrane in macrophages and has been linked to oxidative stress responses.[54] TRPM7 is a Ca^{2+}- and Mg^{2+}-permeable ion channel modulated by $PI(4,5)P_2$ during cellular activation. Interestingly, TRPM7 currents are markedly enhanced by H_2O_2 exposure.[54] In fact, the mRNA and protein expression of TRPM7 are increased in cells exposed to oxidant agents, whereas decreasing TRPM7 levels has been reported to yield a concomitant decrement in intracellular ROS levels,[55] suggesting a positive feedback for TRPM7 activity in an oxidant environment. Thus, the Ca^{2+} overload, increased ROS production, and phosphorylation of ERK and JNK observed in macrophages from *Trpm2*$^{-/-}$ mice may be mediated by increased TRPM7 activity.

In summary, it is clear that regulation of the oxidative stress response by phagocytes is vital for controlling tissue damage in chronic bacterial infections. Here using *H. pylori* as an infection model, we provide novel insight into oxidative stress regulation by phagocytes via the oxidant-activated nonselective cation channel TRPM2. The absence of TRPM2 results in altered calcium homeostasis, and enhanced macrophage production of ROS and inflammatory cytokines associated with increased gastric inflammation in *H. pylori*-infected *Trpm2*$^{-/-}$ mice. The absence of TRPM2 in macrophages stimulates production of inflammatory mediators and promotes classically activated macrophage M1 polarization in response to *H. pylori*. Increased intracellular Ca^{2+} levels in TRPM2$^{-/-}$ macrophages upon *H. pylori* stimulation results in Ca^{2+} overloading, consistent with exacerbated macrophage's inflammatory response. Our data suggest that positive modulation of TRPM2 function may provide a therapeutic strategy to control excessive NADPH-oxidase activity and reduce tissue damage. Alternatively, inhibition of TRPM2 could enhance oxidant-mediated macrophage antimicrobial function during infection.

METHODS

Mice. Mice deficient in TRPM2, C57BL/6J.129 *Trpm2*$^{-/-}$, were generated as described previously.[8] These mice were backcrossed >9 generations at the time of these experiments. WT mice were backcrossed littermate controls housed in the same facilities throughout the experiments. Animals were maintained in the barrier facility at Nationwide Children's Hospital and the Vanderbilt University. Fecal samples were confirmed negative for intestinal *Helicobacter* by PCR (RADIL; IDEXX BioResearch, University of Missouri, Columbia, MO). Feces from sentinel mice housed in the same room were routinely tested by PCR for pinworms, mouse parvovirus, and several other murine pathogens, and consistently tested negative for each of these infections. For all the experiments, 6- to 8-week-old mice were used. The Institutional Animal Care and Use Committees of the Vanderbilt University and the Department of Veteran's Affairs IACUC (V/13/240), and the Research Institute at Nationwide Children's Hospital IACUC (00505AR) approved the animal study protocols.

Culture of *H. pylori*. *H. pylori* strain PMSS1 was used in all experiments. Bacteria were grown on trypticase soy agar plates containing 5% sheep blood. Alternatively, bacteria were grown in Brucella broth containing 5% heat-inactivated fetal bovine serum (FBS) and 10 μg ml^{-1} vancomycin. Cultures were grown at 37 °C in either room air supplemented with 5% CO_2 or under microaerobic conditions generated by a GasPak EZ satchel (BD Diagnostics, Franklin Lakes, NJ, USA).

***H. pylori* infection and tissue harvest**. *Helicobacter*-free *Trpm2*$^{-/-}$ and WT mice, 8–10 weeks old, were used in all *in vivo* experiments. One day before infection of mice, *H. pylori* was inoculated into liquid medium and were cultured for 18 h under microaerobic conditions, as described above. Mice were orogastrically inoculated with a suspension of 5×10^8 CFU (colony-forming unit) *H. pylori* (in 0.5 ml of Brucella broth) two times over 5 days. For 48 h time points, mice received one dose of PMSS1. At animal killing, tissues were collected for various analyses including flow cytometry, cytokine expression analysis, histology (inflammation scoring), and isolation of gastric macrophages.

Processing of mouse stomach tissue. The stomach was removed from each mouse by excising between the esophagus and the duodenum. The forestomach was discarded. The glandular stomach was opened, rinsed gently in cold phosphate-buffered saline (PBS), and cut into three longitudinal strips that were used for bacterial culture, RNA analysis, and histology. For culturing of *H. pylori* from the stomach, gastric tissue was placed into Brucella broth–10% FBS for immediate processing. Gastric tissue was stored in RNALater solution for subsequent RNA isolation.

Histology and immunofluorescence. A longitudinal strip from the greater curvature of the stomach was excised and placed in 10% normal buffered formalin for 24 h, embedded in paraffin, and processed routinely for hematoxylin and eosin staining or immunofluorescence staining. Double-labeled immunofluorescence was carried out to localize F4/80 and iNOS expression in murine stomach. Samples were fixed with 2% paraformaldehyde for 15 min at room temperature. Tissue samples were then incubated overnight at 4 °C with a biotin anti-mouse F4/80 antibody (1:150; Abcam, Cambridge, UK) and a polyclonal rabbit anti-mouse iNOS antibody (1:200; Santa Cruz Biotechnology, Santa Cruz, CA). Alexa Fluor 568 anti-mouse IgG and streptavidin–fluorescein isothiocyanate conjugates were used as secondary antibodies. Samples were mounted using Prolong Gold antifade reagent (Invitrogen, Thermo Fisher Scientific, Carlsbad, CA). Samples were analyzed using the Zeiss 510 LSM Meta confocal laser scanning microscope and Zeiss LSM Image Browser program (Carl Zeiss, Hudson, OH).

Indices of inflammation and injury were scored by a single pathologist (MP) who was blinded to the identity of the mice. Acute

and chronic inflammation in the gastric antrum and corpus were graded on a 0–3 scale. Acute inflammation was graded based on density of neutrophils and chronic inflammation was graded based on the density of lamina propria mononuclear cell infiltration independent of lymphoid follicles. The total inflammation score is the sum of the chronic and acute inflammation scores in the antrum and the corpus.

Gastric macrophage isolation. For gastric macrophage isolations, the stomach removed from each mouse as described above. To dissociate the gastric tissue, the glandular stomach was cut with scissors into 2-mm pieces and digested for 20 min with 1 mg ml^{-1} dispase, 0.25 mg ml^{-1} collagenase A, and 25 U ml^{-1} DNase (Roche Diagnostics, Indianapolis, IN) at 37 °C. The suspension was passed through a 70-μm cell strainer (BD Biosciences, San Diego, CA). Cells were harvested by centrifugation and washed with PBS containing 4% FBS. F4/80^{+} cells were isolated using the MACS Technology (Miltenyi Biotech, Boston, MA). In brief, cells were labeled with biotin-conjugated anti-mouse F4/80 antibody (CALTAG Laboratories, Burlingame, CA). Cells were washed and incubated with streptavidin-conjugated magnetic beads. Cells were brought to a volume of 1 ml with cold MACS buffer, and cell suspensions were applied to a MACS column according to the manufacturer's instructions. The positive fraction was resuspended in DMEM (Dulbecco's modified Eagle's medium) cell culture medium without L-Arg, phenol red, or serum. In some experiments, the positive fraction was incubated with fluorescein isothiocyanate-conjugated monoclonal antibody to the leukocyte marker CD11b and allophycocyanin-conjugated monoclonal antibody to Gr-1, a marker for granulocytes. Cells were analyzed by flow cytometry to determine the percentage of positive cells using a BD Biosciences LSR II system (BD Biosciences). Less than 2% were neutrophils. This procedure consistently leads to close to 90% macrophages (87–92%) as reported previously.[56] Total RNA was isolated using a Versagene 96-well RNA Purification Kit (Gentra Systems, Minneapolis, MN) according to the manufacturer's instructions. cDNA was synthesized from RNA with an iScript cDNA Synthesis Kit (Bio-Rad, Hercules, CA). Three microliters of cDNA was used for a qRT-PCR for *iNOS*, *Arg1*, *Arg2*, *Il1b*, *YM-1*, and *Gapdh*.

Flow cytometric analysis of gastric cellular infiltrates. Whole mouse stomachs were harvested and processed using Miltenyi's Gentle Dissociator (Miltenyi Biotec). In brief, the stomach was cut into 5 mm pieces and then transferred to a C-tube (Miltenyi Biotec) in 5 ml RPMI/10% FBS. The preset Miltenyi Biotec program m_imptumor 02 was run once and then the tissue was digested for 30 min at 37 °C in a solution containing (0.32 mg ml^{-1} Dispase and 0.30 mg ml^{-1} Collagenase D; Roche Diagnostics) while shaking in a CO_2 incubator. After the 37 °C incubation, 100 U ml^{-1} of DNase (Sigma, St. Louis, MO) was added to each tube and the Miltenyi Gentle Dissociator was run for a second and third time using the preset program m_imptumor 02. The tissue homogenate was passed through a 70 μm cell strainer (BD Biosciences). Cells were harvested by centrifugation, washed, and then live cells were counted by using a hemocytometer and trypan blue exclusion staining. The samples were stained with 2 μg ml^{-1} anti-F4/80, 1.5 μg ml^{-1} anti-Gr1 (clone RB6-8C5), and 2 μg ml^{-1} anti-CD11b (clone M1/70) (all antibodies were purchased from BD Biosciences, and analyzed on a BD Biosciences LSR II flow cytometer (BD Biosciences).

RNA extraction and qRT-PCR. RNA was isolated from the stomach and BMDM was isolated using the TRIZOL isolation protocol combined with the Qiagen RNA easy clean-up protocol. RNA was reverse transcribed using the High Capacity cDNA Reverse Transcription Kit (Applied Biosystems, Foster City, CA). For qRT-PCR, we used the relative gene expression method (relative units = $2^{-\Delta\Delta Ct}$). GAPDH (glyceraldehyde 3-phosphate dehydrogenase) served as the normalizer. All qRT-PCR was performed using a Applied Biosystems StepOne Plus instrument (Thermo Fisher Scientific). Levels of cytokine expression are indicated as relative mRNA levels, based on comparison of tissues or cells from *H. pylori*-infected mice with tissues or cells from uninfected mice (calibrator tissue). Taqman Gene Expression Assay primer and probe sets were purchased from Applied Biosystems. Specific primers' GenBank accession number and assay ID are provided in **Supplementary Table 1**. For TRPM2, PCR reactions were performed using the specific primer pair mTRPM2 3380 sense, 5′-CAGATCCCAACCTACATTGACG-3′ and mTRPM2 3594 antisense, 5′-GAAGGTGTAGTTGAACATGGCGA-3′. A 215-bp TRPM2-PCR product was detected after 30 cycles of amplification: 30 s at 94 °C, annealing for 30 s at 46 °C, and extension for 40 s at 72 °C, followed by a final extension for 10 min. For GADPH, PCR reactions used the specific primer pair mGADPH 563 sense, 5′-ACCACAG TCCATGCCATCAC-3′ and mGADPH 1014 antisense, 5′-TCCACC ACCCTGTTGCTGTA-3′. A 451-bp GADPH-PCR product was detected after 30 cycles of amplification: 30 s at 94 °C, annealing for 30 s at 53 °C, and extension for 40 s at 72 °C, followed by a final extension for 10 min.

Culture of *H. pylori* from mouse stomach. Gastric tissue was homogenized using a tissue tearor Biospec (BioSpec Products, Bartlesville, OK). Serial dilutions of the homogenate were plated on trypticase soy agar plates containing 5% sheep blood, 10 μg ml^{-1} nalidixic acid, 100 μg ml^{-1} vancomycin, 2 μg ml^{-1} amphotericin, and 200 μg ml^{-1} bacitracin. After 5–7 days of culture under microaerobic conditions, *H. pylori* colonies were counted.

Preparation and stimulation of BMDM. BMDMs were generated from femurs and tibias of *Trpm2*$^{-/-}$ and WT mice. BM cells were cultured in RPMI-1640 supplemented with 10% FBS, 100 U ml^{-1} penicillin, 100 μg ml^{-1} streptomycin, 2 mM L-glutamine, with the addition of 20% L929 cell-conditioned medium. After 5–7 days of culture, cells were seeded into 6-well tissue culture-treated plates at a density of 2×10^6 cells per well in antibiotic-free medium overnight before infection. Macrophages were infected with live *H. pylori* strain PMSS1 at a multiplicity of infection (MOI) of 10–100 bacteria per macrophage, as indicated. When indicated, macrophages were stimulated with 100 ng ml^{-1} LPS and 20 ng ml^{-1} IFN-γ, or 20 ng ml^{-1} IL-4 and 20 ng ml^{-1} IL-13. After incubation for the indicated time points, culture supernatants and cells pellets were collected and assayed as indicated.

Bactericidal assay. Infected BMDMs with *H. pylori* at an MOI of 10 for 1 h at 37°C were washed two times with PBS, and incubated for 0.5, 1, 2, and 4 h in fresh medium containing gentamicin (100 μg ml^{-1}) to limit the growth of extracellular bacteria. After washing, macrophages were lysed in 1% Triton X-100/PBS for 2 min at room temperature, and centrifuged at 1,000 *g* for 10 min at 4 °C Bacteria were pelleted from the resulting supernatant by centrifugation at 10,000 *g* for 10 min, resuspended in 20 μl of TBS, and kept on ice. Bacteria viability was determined with the LIVE/DEAD BacLight Bacterial Viability Kit (Molecular Probes, Eugene, OR), according to the manufacturer's specifications, and samples were promptly read on a BD Biosciences LSR II flow cytometer. Data for side scattering, forward scattering, and fluorescence were acquired and analyzed with FlowJo software (FlowJo, Ashland, OR).

Measurement of ROS production. BMDMs were plated in nontissue culture-treated 12-well dishes and stimulated with *H. pylori* at different MOIs for 4 h. Culture medium was removed, cells were washed with PBS, and then incubated with CellROX Green reagent (Thermo Fisher Scientific) at 5 μM final concentration in complete RPMI-1640 medium (Invitrogen) for 30 min at 37 °C. For DPI assay, cells were incubated in the presence of 10 μM DPI for 1 h before and during the incubation with *H. pylori*. Cells were washed with warmed PBS (37 °C), removed from plates with cold PBS containing 1 mM EDTA by pipetting, pelleted at 1,500 r.p.m. for 3 min, immediately resuspended in cold PBS containing 1% FBS, and subjected to flow cytometry analysis. Unstained controls were treated similarly, except that

treatments and dyes were omitted. To control for baseline dye fluorescence, samples from each experiment were left unstimulated but stained according to the above procedure. As an alternative method for ROS detection, BMDMs were loaded for 30 min at 37 °C with dihydro-rhodamine 123 (Thermo Fisher Scientific) and stimulated for 30 min at 37 °C with *H. pylori* at different MOIs, 1 μM phorbol 12-myristate 13-acetate, or 100 μM H_2O_2, as indicated. The production of ROS was quantified via flow cytometry by measurement of intracellular rhodamine. Flow cytometry data were acquired on a BD Biosciences LSR II flow cytometer and analyzed using the FlowJo software. Results are presented as the mean channel fluorescence and were normalized to the untreated WT mice. Error bars were generated by calculating s.e.m. from triplicate samples.

Western blot analysis. BMDMs were stimulated with LPS plus IFN-γ, IL-4 plus IL-13, or *H. pylori* (MOI of 10), as indicated. When indicated, cells were pretreated with DPI (10 μM). Cells were washed two times with cold PBS, and then lysed in ice-cold modified RIPA buffer (50 mM Tris-HCl, pH 7.4, 1% Nonidet P-40, 0.5% sodium deoxycholate, 150 mM $NaCl_2$) containing protease inhibitors and phosphatase inhibitor cocktail set (Sigma). Proteins were separated by sodium dodecyl sulfate-polyacrylamide gel electrophoresis and transferred to nitrocellulose membranes. The membranes were incubated with primary antibodies at 4 °C overnight, washed with TRI-buffered saline, including 0.1% Tween-20, exposed to peroxidase-conjugated secondary antibodies for 1 h at room temperature, washed, and then visualized using an Enhanced Chemiluminescence Plus Kit (Thermo Fisher Scientific). Expression of iNOS, Arg1, and β-actin was determined using iNOS-specific antibody and Arg1-specific antibody. Activation of Erk, p38, and JNK was determined using phospho-ERK1/2-, p38-, and phospho-JNK-specific antibody. The total amount of ERK2 and p38 was detected by using ERK2- and p38-specific antibody, respectively. Description of the antibodies used for western blot is provided in **Supplementary Table 2**.

Intracellular Ca^{2+} measurement by flow cytometry. BMDMs were resuspended in cell-loading media (Hank's balanced salt solution with Ca^{2+} and $MgCl_2$ + 1% FBS + 4 mM probenecid) at 1×10^7 cells per ml. The cells were incubated at 37 °C for 30 min with Fluo-3AM (4 μg ml^{-1}) (Molecular Probes), washed two times, and resuspended in cell-loading Ca^{2+}-free medium at 1×10^6 cells per ml. Cells were stimulated with *H. pylori* (MOI of 100), $CaCl_2$ (2 mM), $MgCl_2$ (1.5 mM), or ionomycin (1 μM) (Sigma). The accumulation of intracellular Ca^{2+} in individual cells was assessed by flow cytometry measurement of the fluorescence emission of Fluo-3AM in over 200 s. Data were analyzed using FlowJo's kinetics platform (FlowJo, Ashland, OR).

Electrophysiological recordings. Whole-cell patch-clamp recording was performed on BMDM obtained from WT and *Trpm2*$^{-/-}$ mice, using the same internal solution, Hank's buffer, recording protocols, and the setup as described previously.[57] In voltage-clamp recording, the cells were initially held at −80 mV, given 200 ms voltage episodes in 10 mV increment from −100 to +100 mV, and then the *I–V* relationship was obtained. The capacitance and membrane potentials under the current-clamp mode were also measured.

For *H. pylori*-induced TRPM2 currents in WT macrophages (**Figure 6c,d**), the extracellular solution contained (in mM) 140 NaCl, 2.8 KCl, 1 CaC_2, 1 $MgCl_2$, 10 HEPES-NaOH, and 11glucose. For the intracellular solution (in mM) 130 Cs-glutamate, 8 NaCl, 10 HEPES-CsOH, and 1 $MgCl_2$ were used. Patch-clamp experiments were performed under whole-cell configuration at 21–25 °C using an HEKA EPC10 amplifier (HEKA Instruments, Holliston, MA). Voltage ramps of 100 ms duration spanning from –100 to + 100 mV were delivered at a rate of 0.5 Hz from a holding potential of 0 mV. Currents were normalized to cell size in pF. Data points for inward and outward current amplitudes were obtained at –80 and + 80 mV, respectively. Currents were normalized to the current obtained before development of current activation.

Statistical analysis. Four to 13 mice per group per time point were used for all of the studies. To compare results obtained with different groups of mice, statistical analysis was performed using analysis of variance followed by a Student's unpaired *t*-test. For analyses of bacterial numbers, the data were normalized by log transformation before statistical analysis. For histology scores, the Mann–Whitney *U*-test was applied to compare results between *Trpm2*$^{-/-}$ and WT mice. Statistical analyses were performed using the GraphPad Prism software (GraphPad, La Jolla, CA).

SUPPLEMENTARY MATERIAL is linked to the online version of the paper at http://www.nature.com/mi

ACKNOWLEDGMENTS

We thank Nationwide Children's Hospital and Vanderbilt University's Flow Cytometry and Histology Core Facilities. This work was supported by the National Institutes of Health, NIAID R01-AI092117 (to SP-S) and by Merit Review Grants from the Office of Medical Research, Department of Veterans Affairs. IBX000915A to HMSA and I01BX001453 to KTW. RC is supported by NIAID 1K01AT007324-01, D-LK is supported by K01CA154758-01A1, and KTW is also supported by NIDDKD R01DK053620.

AUTHOR CONTRIBUTIONS

SB, HMSA, and SP-S conceived and designed the project. SB, JNR, RC, MBP, DJH, HC, YG, BD and IL performed experiments. CG, IL, D-LTK and KTW contributed in designing and supervising experiments. SB, HMSA and SP-S wrote the manuscript. All authors discussed and reviewed the manuscript.

DISCLOSURE

The contents in this study do not represent the views of the US Department of Veterans Affairs or the United States Government. The authors declared no conflict of interest.

REFERENCES

1. Freedman, B.D. Mechanisms of calcium signaling and function in lymphocytes. *Crit. Rev. Immunol.* **26**, 97–111 (2006).
2. Feske, S. Calcium signalling in lymphocyte activation and disease. *Nat. Rev. Immunol.* **7**, 690–702 (2007).
3. Randriamampita, C., Bismuth, G. & Trautmann, A. Ca(2+)-induced Ca^{2+} release amplifies the Ca^{2+} response elicited by inositol trisphosphate in macrophages. *Cell Regul* **2**, 513–522 (1991).
4. Desai, B.N. & Leitinger, N. Purinergic and calcium signaling in macrophage function and plasticity. *Front. Immunol.* **5**, 580 (2014).
5. Feske, S., Wulff, H. & Skolnik, E.Y. Ion channels in innate and adaptive immunity. *Annu. Rev. Immunol.* **33**, 291–353 (2015).
6. Perraud, A.L. *et al.* ADP-ribose gating of the calcium-permeable LTRPC2 channel revealed by Nudix motif homology. *Nature* **411**, 595–599 (2001).
7. Sano, Y. *et al.* Immunocyte Ca^{2+} influx system mediated by LTRPC2. *Science* **293**, 1327–1330 (2001).
8. Yamamoto, S. *et al.* TRPM2-mediated Ca^{2+} influx induces chemokine production in monocytes that aggravates inflammatory neutrophil infiltration. *Nat. Med.* **14**, 738–747 (2008).
9. Sumoza-Toledo, A., Fleig, A. & Penner, R. TRPM2 channels are not required for acute airway inflammation in OVA-induced severe allergic asthma in mice. *J. Inflamm. (Lond)* **10**, 19 (2013).
10. Kashio, M. *et al.* Redox signal-mediated sensitization of transient receptor potential melastatin 2 (TRPM2) to temperature affects macrophage functions. *Proc. Natl. Acad. Sci. USA* **109**, 6745–6750 (2012).
11. Di, A. *et al.* The redox-sensitive cation channel TRPM2 modulates phagocyte ROS production and inflammation. *Nat. Immunol.* **13**, 29–34 (2012).
12. Heiner, I. *et al.* Expression profile of the transient receptor potential (TRP) family in neutrophil granulocytes: evidence for currents through long TRP channel 2 induced by ADP-ribose and NAD. *Biochem. J.* **371**, 1045–1053 (2003).

13. Massullo, P., Sumoza-Toledo, A., Bhagat, H. & Partida-Sanchez, S. TRPM channels, calcium and redox sensors during innate immune responses. *Semin. Cell Dev. Biol.* **17**, 654–666 (2006).
14. Sumoza-Toledo, A. *et al.* Dendritic cell maturation and chemotaxis is regulated by TRPM2-mediated lysosomal Ca^{2+} release. *FASEB J.* **25**, 3529–3542 (2011).
15. Haraguchi, K. *et al.* TRPM2 contributes to inflammatory and neuropathic pain through the aggravation of pronociceptive inflammatory responses in mice. *J. Neurosci.* **32**, 3931–3941 (2012).
16. Knowles, H. *et al.* Transient receptor potential melastatin 2 (TRPM2) ion channel is required for innate immunity against *Listeria monocytogenes*. *Proc. Natl. Acad. Sci. USA* **108**, 11578–11583 (2011).
17. Algood, H.M. & Cover, T.L. *Helicobacter pylori* persistence: an overview of interactions between *H. pylori* and host immune defenses. *Clin. Microbiol. Rev.* **19**, 597–613 (2006).
18. Naito, Y. & Yoshikawa, T. Molecular and cellular mechanisms involved in *Helicobacter pylori*-induced inflammation and oxidative stress. *Free Radic. Biol. Med.* **33**, 323–336 (2002).
19. Mantovani, A., Sozzani, S., Locati, M., Allavena, P. & Sica, A. Macrophage polarization: tumor-associated macrophages as a paradigm for polarized M2 mononuclear phagocytes. *Trends Immunol.* **23**, 549–555 (2002).
20. Martinez, F.O. *et al.* Genetic programs expressed in resting and IL-4 alternatively activated mouse and human macrophages: similarities and differences. *Blood* **121**, e57–e69 (2013).
21. Harris, P.R. *et al.* Recombinant *Helicobacter pylori* urease activates primary mucosal macrophages. *J. Infect. Dis.* **178**, 1516–1520 (1998).
22. Gobert, A.P. *et al. Helicobacter pylori* heat shock protein 60 mediates interleukin-6 production by macrophages via a toll-like receptor (TLR)-2-, TLR-4-, and myeloid differentiation factor 88-independent mechanism. *J. Biol. Chem.* **279**, 245–250 (2004).
23. Wilson, K.T. & Crabtree, J.E. Immunology of *Helicobacter pylori*: insights into the failure of the immune response and perspectives on vaccine studies. *Gastroenterology* **133**, 288–308 (2007).
24. Mizuno, T. *et al.* Interleukin-17 levels in *Helicobacter pylori*-infected gastric mucosa and pathologic sequelae of colonization. *World J. Gastroenterol.* **11**, 6305–6311 (2005).
25. Handa, O., Naito, Y. & Yoshikawa, T. Redox biology and gastric carcinogenesis: the role of *Helicobacter pylori*. *Redox Rep.* **16**, 1–7 (2011).
26. Cross, A.R. & Jones, O.T. The effect of the inhibitor diphenylene iodonium on the superoxide-generating system of neutrophils. Specific labelling of a component polypeptide of the oxidase. *Biochem. J.* **237**, 111–116 (1986).
27. Bulua, A.C. *et al.* Mitochondrial reactive oxygen species promote production of proinflammatory cytokines and are elevated in TNFR1-associated periodic syndrome (TRAPS). *J. Exp. Med.* **208**, 519–533 (2011).
28. Naik, E. & Dixit, V.M. Mitochondrial reactive oxygen species drive proinflammatory cytokine production. *J. Exp. Med.* **208**, 417–420 (2011).
29. Bedard, K. & Krause, K.H. The NOX family of ROS-generating NADPH oxidases: physiology and pathophysiology. *Physiol. Rev.* **87**, 245–313 (2007).
30. Griendling, K.K., Sorescu, D., Lassegue, B. & Ushio-Fukai, M. Modulation of protein kinase activity and gene expression by reactive oxygen species and their role in vascular physiology and pathophysiology. *Arterioscler. Thromb. Vasc. Biol.* **20**, 2175–2183 (2000).
31. Bhattacharyya, A. *et al.* Mitogen-activated protein kinases and nuclear factor-kappaB regulate *Helicobacter pylori*-mediated interleukin-8 release from macrophages. *Biochem. J.* **368**, 121–129 (2002).
32. Pathak, S.K. *et al.* TLR4-dependent NF-kappaB activation and mitogen- and stress-activated protein kinase 1-triggered phosphorylation events are central to *Helicobacter pylori* peptidyl prolyl *cis-*, *trans*-isomerase (HP0175)-mediated induction of IL-6 release from macrophages. *J. Immunol.* **177**, 7950–7958 (2006).
33. Zhao, Y. *et al. Helicobacter pylori* heat-shock protein 60 induces interleukin-8 via a Toll-like receptor (TLR)2 and mitogen-activated protein (MAP) kinase pathway in human monocytes. *J. Med. Microbiol.* **56**, 154–164 (2007).
34. Nunez-Villena, F. *et al.* Increased expression of the transient receptor potential melastatin 7 channel is critically involved in lipopolysaccharide-induced reactive oxygen species-mediated neuronal death. *Antioxid. Redox Signal.* **15**, 2425–2438 (2011).
35. Su, L.T. *et al.* TRPM7 activates *m*-calpain by stress-dependent stimulation of p38 MAPK and c-Jun N-terminal kinase. *J. Mol. Biol.* **396**, 858–869 (2010).
36. Inoue, H., Murayama, T., Tashiro, M., Sakurai, T. & Konishi, M. Mg(2+)- and ATP-dependent inhibition of transient receptor potential melastatin 7 by oxidative stress. *Free Radic. Biol. Med.* **72**, 257–266 (2014).
37. Hoth, M. & Penner, R. Depletion of intracellular calcium stores activates a calcium current in mast cells. *Nature* **355**, 353–356 (1992).
38. Feske, S. *et al.* A mutation in Orai1 causes immune deficiency by abrogating CRAC channel function. *Nature* **441**, 179–185 (2006).
39. Vig, M. *et al.* CRACM1 is a plasma membrane protein essential for store-operated Ca^{2+} entry. *Science* **312**, 1220–1223 (2006).
40. Montell, C. The TRP superfamily of cation channels. *Sci. STKE* **2005**, re3 (2005).
41. Hogan, P.G. & Rao, A. Dissecting ICRAC, a store-operated calcium current. *Trends Biochem. Sci.* **32**, 235–245 (2007).
42. Robinson, L.C. & Marchant, J.S. Calcium influx: beyond "current" biology. *Curr Biol* **16**, R548–R550 (2006).
43. Partida-Sanchez, S. *et al.* Chemotaxis of mouse bone marrow neutrophils and dendritic cells is controlled by adp-ribose, the major product generated by the CD38 enzyme reaction. *J. Immunol.* **179**, 7827–7839 (2007).
44. Knowles, H. *et al.* Transient receptor potential melastatin 2 (TRPM2) ion channel is required for innate immunity against Listeria monocytogenes. *Proc. Natl. Acad. Sci. USA* **108**, 11578–11583 (2011).
45. Qian, X. *et al.* Transient receptor potential melastatin 2 protects mice against polymicrobial sepsis by enhancing bacterial clearance. *Anesthesiology* **121**, 336–351 (2014).
46. Wehrhahn, J., Kraft, R., Harteneck, C. & Hauschildt, S. Transient receptor potential melastatin 2 is required for lipopolysaccharide-induced cytokine production in human monocytes. *J. Immunol.* **184**, 2386–2393 (2010).
47. Kim, H.R. *et al.* Reactive oxygen species prevent imiquimod-induced psoriatic dermatitis through enhancing regulatory T cell function. *PLoS One* **9**, e91146 (2014).
48. Efimova, O., Szankasi, P. & Kelley, T.W. Ncf1 (p47phox) is essential for direct regulatory T cell mediated suppression of CD4+ effector T cells. *PLoS One* **6**, e16013 (2011).
49. Brechard, S. & Tschirhart, E.J. Regulation of superoxide production in neutrophils: role of calcium influx. *J. Leukocyte Biol.* **84**, 1223–1237 (2008).
50. Barbet, G. *et al.* The calcium-activated nonselective cation channel TRPM4 is essential for the migration but not the maturation of dendritic cells. *Nat. Immunol.* **9**, 1148–1156 (2008).
51. Foyouzi-Youssefi, R., Petersson, F., Lew, D.P., Krause, K.H. & Nusse, O. Chemoattractant-induced respiratory burst: increases in cytosolic Ca^{2+} concentrations are essential and synergize with a kinetically distinct second signal. *Biochem. J.* **322**, 709–718 (1997).
52. Granfeldt, D., Samuelsson, M. & Karlsson, A. Capacitative Ca^{2+} influx and activation of the neutrophil respiratory burst. Different regulation of plasma membrane- and granule-localized NADPH-oxidase. *J. Leukocyte Biol.* **71**, 611–617 (2002).
53. Gallois, A., Bueb, J.L. & Tschirhart, E. Effect of SK&F 96365 on extracellular Ca^{2+}-dependent $O2^-$ production in neutrophil-like HL-60 cells. *Eur. J. Pharmacol.* **361**, 293–298 (1998).
54. Aarts, M. *et al.* A key role for TRPM7 channels in anoxic neuronal death. *Cell* **115**, 863–877 (2003).
55. Chen, H.C., Su, L.T., Gonzalez-Pagan, O., Overton, J.D. & Runnels, L.W. A key role for Mg(2+) in TRPM7's control of ROS levels during cell stress. *Biochem. J.* **445**, 441–448 (2012).
56. Chaturvedi, R. *et al.* L-arginine availability regulates inducible nitric oxide synthase-dependent host defense against *Helicobacter pylori*. *Infect. Immun.* **75**, 4305–4315 (2007).
57. Gu, Y., Barry, J. & Gu, C. Kv3 channel assembly, trafficking and activity are regulated by zinc through different binding sites. *J. Physiol.* **591**, 2491–2507.